Response to Comments from Referee #1

We thank this reviewer for his/her detailed and insightful comments which are very helpful in our revision of the manuscript. We have made every effort to address all the concerns raised by this review and we hope our efforts will bring our manuscript closer to being accepted for publication on ACP. Our point-by-point response is given below.

General comments: I think that the structure of this paper needs some work. The abstract and methodology completely omit any detail about the range of simulations undertaken or the hypothesis that is being tested. Some of this detail is found in the results section but this means that it comes as something as a surprise when reading. I also think this work could have been presented in a more succinct way. Nineteen figures are probably too many and the structure of the work means that there is a lot of skipping between figures. For a number of figures only 1 or 2 panels are referred to in the text. Specifically, I am unconvinced by the use of 2 m temperature and water vapour mixing ratio. Why not use thermodynamic quantities such as equivalent and virtual potential temperature. These give information about air masses (including temperature and moisture) and buoyancy and could still have important temperature and water vapour contours over plotted as needed. Also, from appearances it seems like NCL has been used for the creation of most figures making the calculation of such variables easy using pre-written scripts such as "wrf_eth" and "wrf_virtual_temp".

R: We thank the reviewer for the detailed suggestions above, which are mostly adopted in the revision. The description of all experiments has now been included in the methodology part, and the abstract has been revised to highlight the key findings of this work. We removed Figs. 15, 16, 17, 19 for the succinctness of the main manuscript. We chose to use 2-m temperature and water vapor mixing ratio instead of equivalent and virtual potential temperature because these potential variables may compound the impacts from radiative heating/cooling versus sources of moisture and transport which we seek to distinguish.

The description of the processes that cause specific features is also lacking in some cases. If the authors have not tested what is driving the production of those features it should be made clear, if they have then say so. Generally, the written English in the manuscript reads well, however, there are a few instances when the wording is slightly odd or does not conform with standard scientific usage. For example, simulations are referred to as being "convection-allowing" when it is more usual to describe them as being "convection permitting". While the intent is clear it should be changed to conform with previously published work. I also found the use of acronyms to be confusing "LSB" could just be referred to as "land-breeze", "DP" could just be "diurnal precipitation" etc.

R: We added more descriptions of specific physical processes in the revised manuscript per recommendation of the reviewer. All "convection-allowing" have now been revised as "convection permitting" throughout the manuscript. We also reduced the use of acronyms for a better readability, for example, "DP" was revised as "diurnal precipitation". We chose to keep the "LSB" as an acronym of "land sea breeze" because it was mentioned too many times and has been used in many papers. For example,

Lo, J.C., Lau, A.K., Fung, J.C. and Chen, F., 2006. Investigation of enhanced cross-city transport and trapping of air pollutants by coastal and urban land-sea breeze circulations. *Journal of Geophysical Research: Atmospheres*, *111*(D14).

Chen, T.C., Yen, M.C., Tsay, J.D., Liao, C.C. and Takle, E.S., 2014. Impact of afternoon thunderstorms on the land–sea breeze in the Taipei Basin during summer: an experiment. Journal of Applied Meteorology and Climatology, 53(7), pp.1714-1738.

Specific comments

Abstract
23 and throughout Change "convection-allowing" to "convection permitting".

R: Changed as suggested.

24-26 Change to "ERA-interim reanalysis. The simulations have a slight overestimation of rainfall amounts and a 1-h delay in peak rainfall time. The diurnal cycle of precipitation is driven by the occurrence of moist convection around noon owing to low-level convergence associated with the sea-breeze circulation"

R: Revised as suggested in lines 27-30.

29 Change to "Generally precipitation dissipates quickly in the evening due to …"

R: Revised as suggested in lines 32-34.

Introduction
Be much clearer about the novel nature of your work. You have cited many other pieces of work that look into similar processes and use similar models, what do you do that hasn't been done elsewhere.

R: The novelty of this current work is that semi-idealized convection-permitting simulations with climatological mean initial conditions and diurnally averaged periodic lateral boundary conditions were used for the first time to study the dynamic and thermodynamic processes (and the impacts of land-sea breeze circulations) that control the rainfall distribution and climatology over a tropical island. This uniqueness has been clarified in the revised introduction.

49 What grid-spacing and model did Hassim et al., (2016) use? Include it here. Hassim looks at the importance of the sea breeze in the initiation of rainfall but focusses on large-scale atmospheric properties preferential to the propagation of systems offshore at night. This is not what you have said here, much more detail is required here.

R: The model and grid spacing used by Hassim et al. (2016) have been added here. We also revised the way we cited Hassim et al (2016) in a clearer way as "Hassim et al. (2016) examined the diurnal cycle of rainfall over New Guinea with a 4-km convection-allowing WRF model. They looked at the importance of the sea breeze in the initiation of rainfall but focused on large-scale atmospheric properties preferential to the propagation of systems offshore at night. They also found that

orography and the coastline along with gravity waves were beneficial for the longevity and maintenance of the convection systems though they were not the fundamental reason for the convection initiation." In Lines 56-62.

50-51 Be specific about what was beneficial about orography and gravity waves. This is not enough detail.

R: More detailed description was added here. Please also refer to our response to the last comment.

52-53 In what way was island size important, how do the findings from these papers relate to the size of Hainan island?

R: This sentence has been removed as our work does not examine impacts of different island sizes.

57 Change to "Diurnal variability is only captured in some places and months where…"

R: Revised as suggested in lines 68-69.

61 There is a long list of references here after a very vague statement, please be much more specific.

R: We have revised this sentence for clarity and removed some of references that were not quite relevant as "Studies show that the LSB may have different contributions to the diurnal variabilities of precipitation at different places (Keenan et al. 1988; Qian 2008; Wapler and Lane 2012; Chen et al. 2017). Precipitation tends to be initiated by the convergence of land breezes (Wapler and Lane 2012) and sea breezes (Qian 2008) over gulf area and islands area, respectively. Interactions between land breeze and prevailing wind are likely to produce precipitation over the coast area or tropical islands (Keenan et al. 1988; Chen et al. 2017)." in lines 70-75.

73-76 This description of Hainan Island seems incongruous. Either remove, or, if this is part of the motivation for the work make it clear what impact your work has on Hainan and how these facts relate to that impact.

R: Those sentences have been removed as suggested.

80 replace "rather" with "more"

R: Revised as suggested in line 91.

87-96 Highlight why this work is unique.

R: We have highlighted the novelty as " This is the first time using semi-idealized convection-permitting simulations with climatological mean initial conditions and diurnally averaged periodic lateral boundary conditions were used for the first time to study the dynamic and thermodynamic

processes (and the impacts of land-sea breeze circulations) that control the rainfall distribution and climatology over a tropical island.". We would also highlight the removal of terrain effect, along with the further simplification using a perfect oval-shaped island. In Lines 99-104.

Observation dataset and methodology

Don't describe the distribution of the gauges as homogeneous. Gauges are discrete with gaps in-between and so can never be homogeneous. Maybe just say they are "relatively evenly distributed across the island"

R: As suggested, this sentence has been changed to "The gauges are relatively evenly distributed across the island." in lines 115-116.

100 Why are they suitable for assessing the diurnal precipitation, what is the sampling frequency? Etc.

R: The sampling frequency is one hour, which is dense enough to represent the diurnal rainfall cycle over the island. We have clarified this in the revised manuscript in lines 116-117.

102 Give an idea of the time period you are talking about how many stations where built after 1951 and say what years new stations became operational. If a single station was built in 1951 and the rest were built in 2009 your current description would still be true. Be more specific!

R: A table is added in the revised manuscript to show the observation period.

Table 1 Information of stations used in this work

Station No.	Latitude	Longitude	Height (m)	Obs period(YearMonth)	Name
59757	20	110.37	9.9	197701-201212	Qiongshan
59758	20	110.25	63.5	195101-201212	Haikou
59838	19.1	108.62	7.6	195506-201212	Dongfang
59842	19.9	109.68	31	196201-201212	Lingao
59843	19.73	110	31.4	195901-201212	Dengmai
59845	19.52	109.58	169	195505-201212	Zanzhou
59847	19.27	109.05	98.1	196605-201212	Changjiang
59848	19.23	109.43	215.6	196201-201212	Baisha
59849	19.03	109.83	250.9	195602-201212	Qiongzhong
59851	19.7	110.33	24.2	196301-201212	Dingan
59854	19.37	110.1	118.3	196301-201212	Tunchang
59855	19.23	110.47	24	195509-201212	Qiaonghai
59856	19.62	110.75	21.7	195901-201212	Wenchang
59940	18.75	109.17	155	196202-201212	Ledong
59941	18.77	109.52	328.5	196301-201212	Wuzhishan
59945	18.65	109.7	68.6	196509-201212	Baoting
59948	18.22	109.58	419.4	196201-201212	Sanya
59951	18.8	110.33	39.9	196201-201212	Wanning
59954	18.5	110.03	13.9	195601-201212	Lingshui

103-110 Please use present tense e.g. “observations are augmented” not “observations were augmented”.

R: The tense has been revised to present tense in line 122.

105 Define NOAA and CMORPH

R: NOAA and CMORPH have been defined as “National Oceanic and Atmospheric Administration (NOAA) and Climate Prediction Center Morphing Technique (CMORPH)” in lines 122-123.

105 CMORPH is a retrieval not an analysis.

R: “...the CMORPH analyses” was changed to “...the CMORPH data” as suggested in line 123.

106-108 delete “as shown to be valuable in past studies of diurnal precipitation over China (e.g. He and Zhang 2010, … Zhang et al., 2014)”

R: Removed as suggested.

108 Change to “The CMORPH grid with a temporal resolution of 30 minutes.

R: Revised as suggested in line 125.

111-121 You need to add a lot more detail about the specific experiments here. What version of WRF is used? Advanced Research WRF would be my assumption but it is not specified. A much greater amount of detail is needed about the schemes that were used with an explanation of why. If they were used to conform to Chen et al (2016) then describe the experiments performed in Chen et al (2016) too. Each of your experiments has to be explained too, “A series of convection-allowing numerical simulations were performed” gives absolutely no detail about what you have done or why!

R: The Advanced Research WRF (ARW) 3.7.1 was used in this study, which has been cited in lines 127-128. Detailed description of all numerical simulations was included in the revised manuscript in lines 133-138 and Lines 142-154. We admit that the choice of WRF schemes is subjective in nature, based primarily on many years of experience of the senior authors, and we did not perform exclusively sensitivity tests to the choice of numerous combinations of different WRF physical parameterization schemes, nor did Chen et al. (2016). However, the realistic rainfall distribution simulated by the control simulation in comparison to climatology gives us confidence that the simulations so designed are well suited for this study.

Observational analysis

136-137 Say that this is the monsoon season.

R: As suggested, the sentence ”Most of the precipitation falls from April to October and exhibits a distinct diurnal cycle during that period” has changed to “Most of the precipitation falls from April to

October, which is the monsoon season, and exhibits a distinct diurnal cycle during that period" in lines 166-168.

149-152 Replace with "No heavy rainfall or distinct diurnal variability is observed at stations along the southern coastline (blue dots on figure 1 and blue lines on figure 2).

R: Replaced as suggested in lines 182-184.

149-165 What is the criteria for the different dot colours? I would assume that you would group them based on some geographical property e.g. southern coast, highlands, plain, northern coast, but it looks instead like they are grouped based on their diurnal cycle, which makes the grouping less useful.

R: We grouped the stations based on their similarity in diurnal variations, which to a large extent are correlated with their geographical locations so they are internally consistent. We chose to keep the station coloring unchanged. We have included this reason in lines 180-182.

157 swap "also are" to "are also"

R: Revised as "were also" in line 189.

162 change to "These results indicate good agreement between CMORPH data and gauges, in particular …"

R: Revised as suggested in lines 194-195.

174 change to "for the whole year and over the whole island"

R: Revised as suggested in line 205.

174-181 You need to highlight that the precipitation levels for panels a, b, c, d, k and l are so low that essentially the diurnal precipitation percentage is meaningless, or, even get rid of those panels.

R: Even though low precipitation occurs during those months, their diurnal cycles can still be important because the small diurnal precipitation amount can be potentially important for plant and vegetation, and air quality. We prefer to keep them for completeness of the annual evolution of diurnal cycles. We nevertheless focus on the May and June months that have the highest diurnal precipitation amount for the rest of the study.

177-178 delete "However, the diurnal precipitation… precipitation intensity." You have just defined this, therefore this is obvious and not needed.

R: Deleted as suggested.

178-181 Even discussing March here seems pointless, March has almost no rainfall, so the magnitude of the diurnal component of almost nothing is not interesting at all. What seems more interesting is that rainfall amounts fall from May to July, increase in August again and then drop into October. However the diurnal percentage drops steadily throughout the season. You mention "physical processes", what are these, be specific! Is it associated with synoptic scale storms, typhoons, prevailing winds? Say what and describe the processes too.

R: For the reasons discussed above, we choose to keep the discussion despite the small amount of total precipitation in March. We do keep the discussion on the low precipitation month brief and focus primarily on May and June months.

Besides the processes listed by the reviewer (synoptic scale storms, typhoons, prevailing winds), other possible mechanisms include changes in the land sea temperature contrast, atmospheric moisture content, which will be explored in our future study. We added a brief discussion giving these physical processes in Lines 213-217.

193 do you mean the Katabatic downhill jet, (which is a component of MPSs) which would happen on both sides of mountains. MPSs (to my understanding) are a feature of the lee side of mountain or plateaus, and given the direction of the prevailing wind it is unlikely that this would have an impact on the southern edge of Hainan.

R: The mountain plain solenoid circulation has been revised as downhill jet circulation in line 229.

196-198 Figure 6 discussed here is not every 3 hours as stated as panel (f) shows 1700, if this is due to this being the peak rainfall time, say this explicitly.

R: The sentence "(every 3 h in Fig. 6)" has been revised as "(every 3 h except using 1700 LST as it is the peak rainfall time in CMORPH observation in Fig. 6)" in lines 232-233.

Numerical simulations.

228-234 This is very clearly lacking a clear description of the simulations that have been conducted as part of this study and the hypotheses that are being tested by performing them. It seems like much of the detail is included later, but this structure is confusing and should be changed.

R: All the description of the simulations has been moved to the observation dataset and methodology section.

240-241 change to "slightly higher peak values of simulated 2-meter temperature and simulated precipitation…"

R: Changed as suggested in lines 269-270.

242 Say "the chosen setup of WRF-ARW has the ability to…"

R: Revised as suggested in lines 271-272.

256 Evening rainfall along southern coast is missing, you should mention this, including why this might be.

R: As suggested, we added a sentence in Lines 286-289 as "However, the evening rainfall along southern coast is missing, which is likely because the resolution we used in this study is still too coarse to resolve the convection over the southern coast or the physical process was so complex that the model is unable to represent it for now".

265-269 This is an experiment setup description and should not be in the results section.

R: The description of the experimental setup has been moved to the observation dataset and methodology section.

310 Fog is not the only potential reason, cold pool air could be colder, what impact does stability have on the formation of fog. It needs more detail of discussion.

R: We agree with the reviewer that fog may not be the only potential reason. Other alternative possible reasons are also given here as "The slower warming in the northeastern part of the Hainan Island is likely due to the morning fog or cold pool air (Fig. 13b) that commonly forms within the area humidified (Fig. 14b) by late-afternoon precipitation on the preceding day. The cloud over the area attenuates solar radiation and subsequently slows the local warming. Moreover, positive horizontal temperature advection exists over the southern island (Fig. 15), which helps to increase the temperature faster over the area." (Lines 340-345). The impact of stability on the formation of fog is not quite relevant to the discussion here and thus not included in the revision.

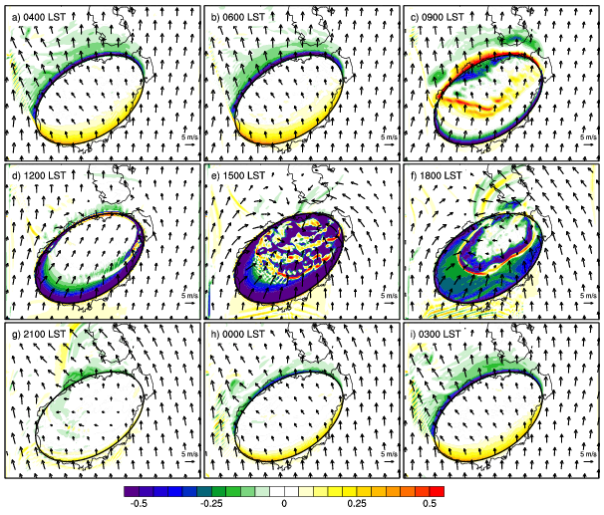

Fig. 15. Horizontal temperature advection (shaded) and horizontal wind (vector) on the first model level.

311 I'm not sure that 14b does show what is stated. Maybe the colour scale of 14b is not appropriate?

R: This figure has been revised with relative humidity (RH) replacing water vapor mixing ratio. Much moister air can be easily observed during the evening and early morning, which is beneficial for the generation of morning fog, cold pool air or others. Below shows the revised Figure 14.

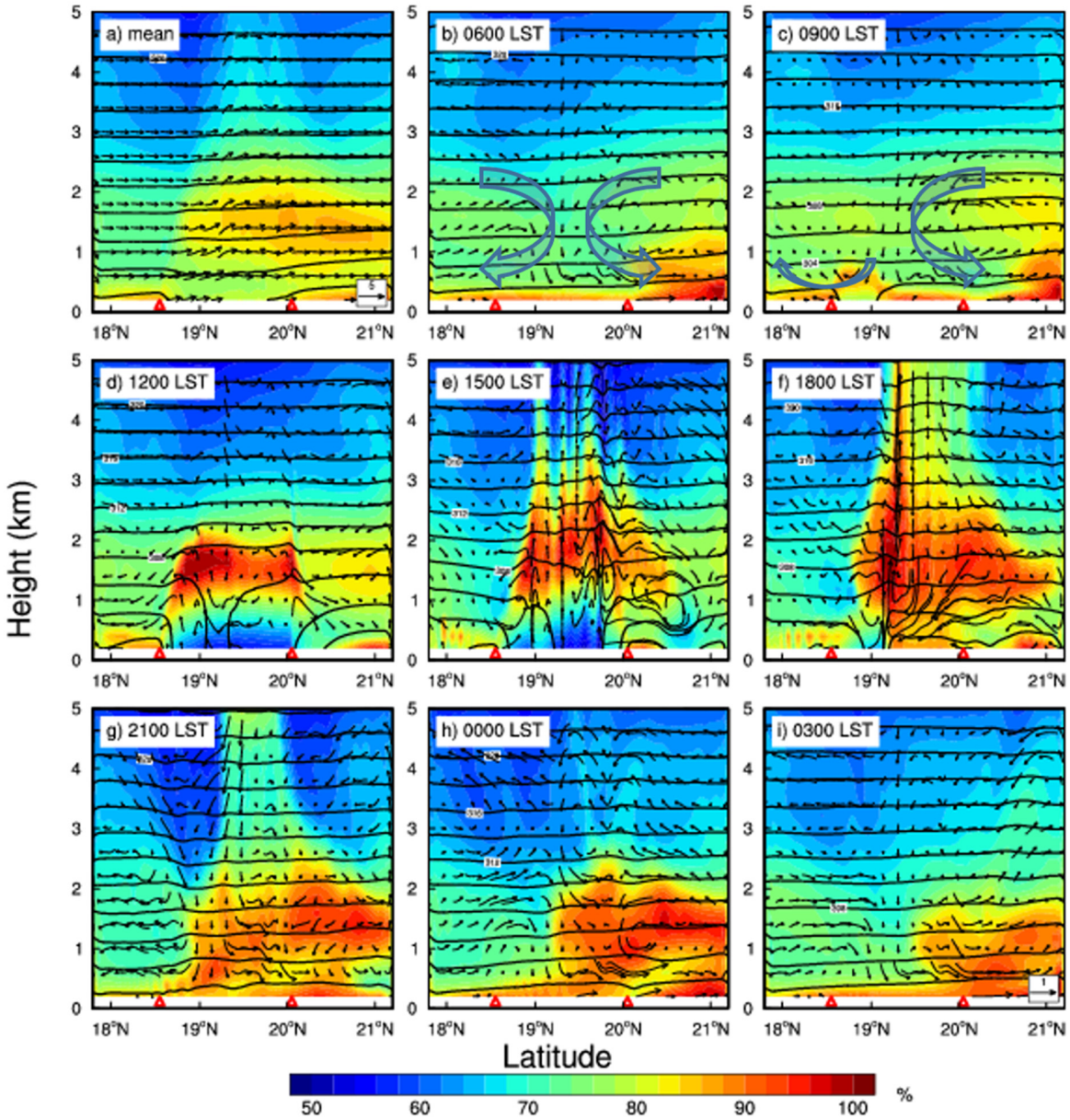

Fig. 14. Vertical cross-sections of relative humidity (shading), perturbation wind (vectors;the scale of the vertical component is increased by a factor of 5), and temperature (contours) in the south-to-north direction (see red line in Fig. 1) averaged over all hours (a) and at 3-h intervals (b–i). The triangles in each panel indicate the edges of the island.

316-318 15b and 15c don't show what you say they do, at 0900 the vectors does show land breezes at both coasts but at 0600 LST only one is clear in the figure.

R: We agree that our original description is not clear. The sentence has been revised as "Two land-breeze circulations (LBCs) appear clearly in the vertical direction below 3 km along the coast of the island at 0600 LST (Fig. 14b). The southern LBC recedes quickly with the reversal of the temperature gradient at around 0900 LST, while the other LBC remains distinct (Fig. 14c)." in lines 348-351. We added arrows marking the locations of the LBCs (below shows the new Fig. 14 with the LBCs in b and c).

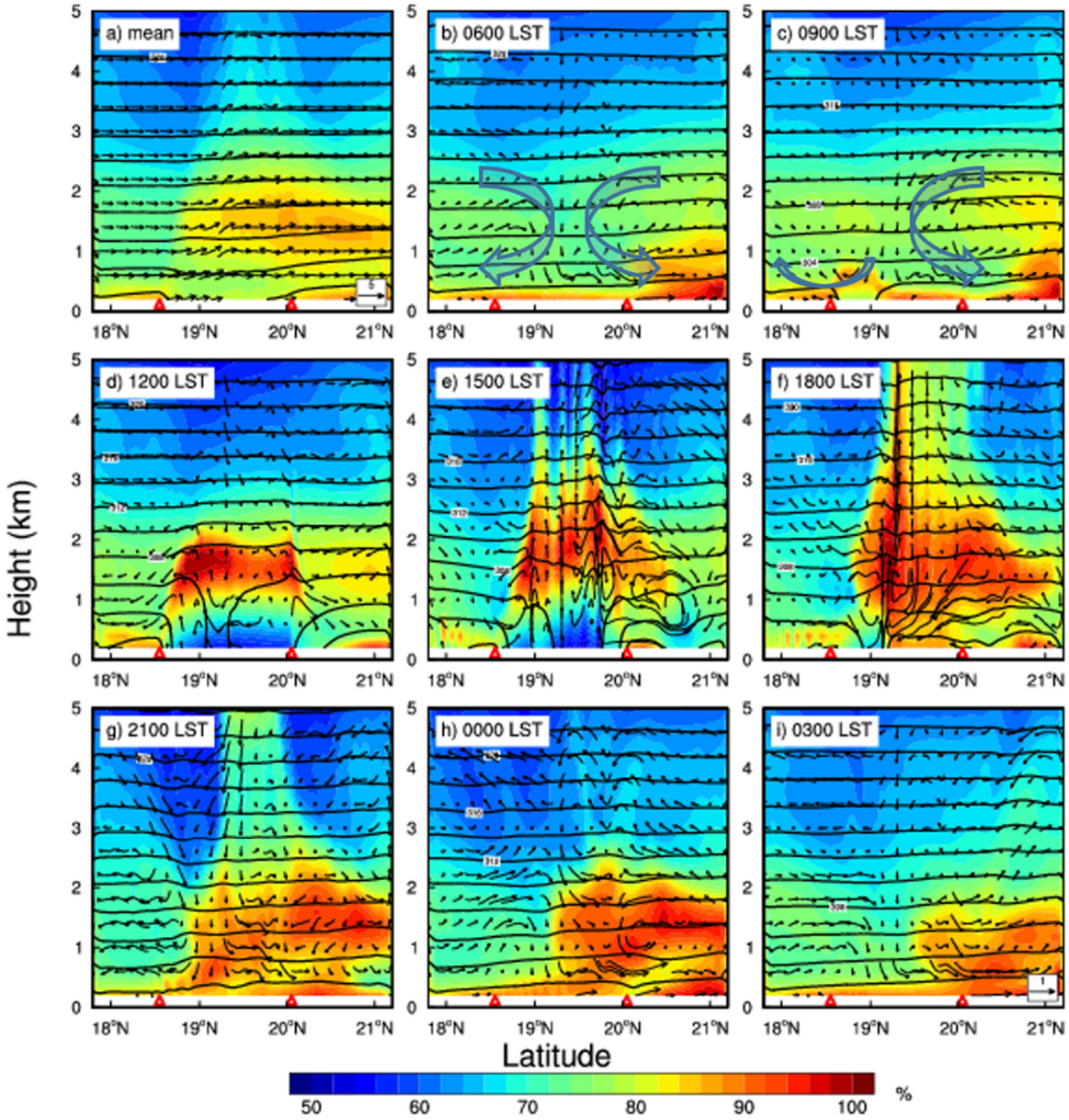

Fig. 14. Vertical cross-sections of relative humidity (shading), perturbation wind (vectors; the scale of the vertical component is increased by a factor of 5), and temperature (contours) in the south-to-north

direction (see red line in Fig. 1) averaged over all hours (a) and at 3-h intervals (b–i). The triangles in each panel indicate the edges of the island.

319-325 The region that at 0900 LST had suppressed 2m temperatures has elevated 2 m temperatures at 1200 LST. You do not give an explanation for such rapid warming in one part of the domain while other areas (also over land have more gradual warming). I cannot work out what the cause might be from this work.

R: The unevenly warming temperature over the island is a result of the horizontal temperature advection, which was demonstrated in new Figure 15 showing horizontal temperature advection with the horizontal wind on the lowest model level. From the evening to the early morning (2100-0600 LST), the temperature over the island is lower than the surrounding ocean, then the temperature along the south coastlines will increase faster than the other area as affected by positive horizontal temperature advection. After 0900 LST, the temperature over the island is warmer than the surrounding ocean, so the temperature will increase slower along the coast as affected by the negative horizontal temperature advection. It is just the opposite phenomenon along the north coastline areas that affected by negative temperature advection during the evening to early morning and positive temperature advection at other times. This reason and the new Figure 15 have been added in the revised manuscript in Lines 352-364.

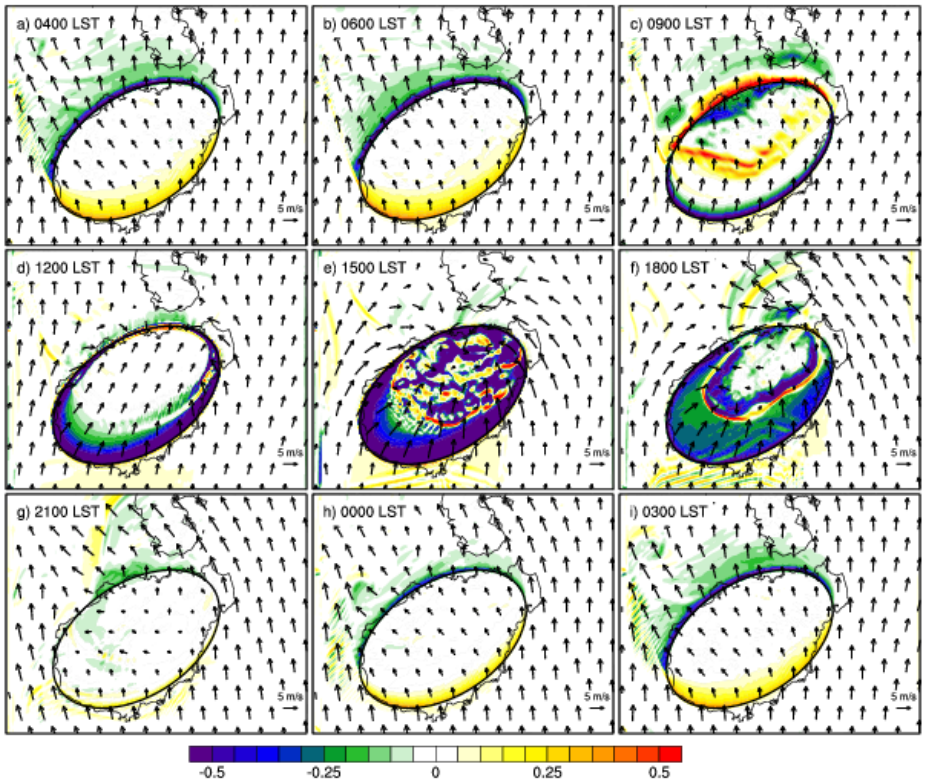

Figure 15. Horizontal temperature advection (shaded) and horizontal wind (vector) on the first model level.

338 I don't believe that the deep prevailing wind is what gives that moisture pattern seen in 11e. This looks a lot more like what one would expect from low level convergence of moist air producing updraughts.

R: We agree. The sentence has been revised as "Moisture air is transported from ocean to the island persistently by the deep southwesterly prevailing wind throughout the lower troposphere (Fig.11e) while low level convergence of moist air generates strong updraughts, which results in an increase of the moisture over the midlevels (Fig. 14e)." in lines 377-380.

354 Quote numbers, specifically the times at which this occurs and rates.

R: We revised the sentence as "The rate of temperature decrease is fastest in the first several hours during this stage, reaching around -1.5 K/h during 1800-1900 LST (red line in Fig. 7d)" in lines 396-397.

361-364 Drying at 850 hPa and in cross section seems predominantly driven by downward limb of the circulation advecting dry air from aloft. Movement of moisture over the northern coast also seems to be much more likely associated with the dominant wind direction than land breezes.

R: We agree. The drying at 850 hPa was attributed to the downward flow as stated in lines 406-408. Movement of moisture over the northern coast was also attributed to the dominant wind direction than land breezes as stated in Lines 408-410.

377-382 Description of simulation should not be in results.

R: Description of simulation has been moved to "Observation dataset and methodology" section.

402-403 This statement needs investigation, how does the presence of a cold pool enhance inland penetration of the sea-breeze? What are the dynamics of the situation and what have you shown to support your assertion.

R: When a cold pool moves toward the island/inland, the pressure gradient should increase which drives the flow more inland.

Summary

Summary needs to include the results above that I have said are lacking. Greater specificity and inclusion of the implications of this work in the broader context of previous and ongoing work.

R: The conclusion part has been revised as suggested. In particular, main findings as summarized by this reviewer in his/her general comment are summarized. (1) WRF is capable (in this setup) of replicating the important aspects of the mean diurnal cycle compared to rainfall observations, (2) That removing the orography and coastal features made little difference to the diurnal cycle during the rainiest times of the year, (3) the dominant process that produces the diurnal cycle were shown to be the sea/land breezes caused by the relative surface heating/cooling of the island compared to the surrounding ocean and (4) that evaporative cooling as part of convective systems also plays an important role in the diurnal cycle. Those have been concluded in lines 488-494.

425 Boundary conditions cannot be cyclic, they come from averaged ERA-Interim data! Do you mean lateral boundary conditions?

R: Thanks for this correction. The "cyclic boundary conditions" has been revised as "cyclic lateral boundary conditions" in lines 481-482.

Figures

Latitude and Longitude should be marked on all maps and along the cross sections.

R: All the map and cross section figures have been added with latitude and longitude.

F2 Units should be mm hr^{-1}

R: The units has been revised as "mm h^{-1}"

F3 Units cannot just be mm. This has to be a rate mm hr^{-1}? The caption is also not clear enough "Diurnal cycles of hourly average rainfall accumulations obtained from …"

R: The units has been revised as "mm h^{-1}", and the caption has been revised as "Diurnal cycles of hourly average rainfall accumulations obtained from gauges (blue) and CMORPH (red) in each month".

F4 This is a confusing figure given that we know that rainfall totals are inconsequential in panels a,b,c,d,k and l. More useful just to show months May-October when some rain actually falls. Also Caption and text refers to percentage, I think the values are not expressed as such given the range between 0.1 and 0.95.

R: As we discussed in response above, even though the rainfall is quite small, the percentage of the diurnal precipitation is still quite important. We choose to keep those panels. The caption has been revised as "Percentage of the total precipitation that can be attributed to the diurnal cycle…..".

F5 Units should be mm hr^{-1}

R: Revised as suggested.

F6 Units should be mm hr^{-1} and numbers on scale are vertically squashed.

R: The units has been revised as "mm h^{-1}". The numbers on scale were revised to have a normal look.

F7 Get rid of the horizontal mean lines, they are not very useful and make the plots more confusing.

R: Removed as suggested.

F8,9,10,11,12,13,14,15,16,17 and 19 The comparison between (f) panels with F6 is at a different time. This doesn't have to change but it should be made clearer in the text that this discrepancy in comparison is present.

R: We have clarified this discrepancy in the text.

F13 seems almost entirely pointless as a figure. It seems like the authors have tried out some new visualisation software and were very keen to include a figure using the resultant images without considering what it is that they were trying to show with such an image. It is difficult to interpret and the colours on the only panel referred to (b) are almost impossible to distinguish.

R: We chose to keep this figure to give a good big picture of the relationship between multiple variables including the 2-m temperature, wind perturbation, cloud and precipitation feature.

F18 Need to include information about approximate height above the surface of the second model level, both in caption and in main text.

R: The height if the second model level has been added in the caption and main text. The second lowest model level is the 0.994-sigma level, which is about 50 m above the surface.

Response to Comments from Referee #2

We thank this reviewer for his/her detailed and insightful comments which are very helpful in our revision of the manuscript. We have made every effort to address all the concerns raised by this review and we hope our efforts will bring our manuscript closer to being accepted for publication on ACP. Our point-by-point response is given below.

Major comments:

1. A numerical sensitivity experiment (FakeDry) is used to demonstrate the impact of cold pool on the sea breeze. In this FakeDry run, all latent heating and cooling is turned off. This prevents both diabatic feedback from the latent heat of condensation in the whole troposphere and cold pool due to rain re-evaporation in the lowest 1-2 km. Both can be responsible for the difference between FakeDry and the control run. So, conclusions (e.g., line 28-29, Line 446-449) from this FakeDry experiment regarding the role of cold pool may be revised. Otherwise, another experiment turning off rain re-evaporation in the lowest 1-2 km may be conducted to further clarify the exclusive roles of cold pool versus diabatic heating throughout the troposphere.

R: Another sensitivity experiment NOVAP which turns off rain re-evaporation has been conducted as suggested. Comparing rainfall and the propagation of sea breeze among the experiments IDEAL, FakeDry and NOVAP, we found that the propagation speed in NOVAP is in the middle of the IDEAL and FakeDry, which means that the cold pool can speed up the propagation. Also, it can be found that the precipitation intensity is much greater in NOVAP, indicating that the cold pool can suppress the precipitation significantly. The description of NOVAP experiment has been included in the "Observation dataset and methodology" part. The results and comparison of the experiments have been included in "The impacts of latent heating/cooling on LSB and the related rainfall" part.

Specific comments:

Line 45: it is stated that "precipitation is usually due to convection". What else could rain come from other than convection?

R: The sentence has been revised as "Tropical precipitation is usually due to convection" in line 49.

Line 101: "full" records?

R: Revised as suggested. The sentence "though records exist ..." has been revised as "though full records exist ..." in line 118.

Lines 112-113: What are the surface boundary conditions? Is surface temperature predicted over both land and sea, or just predicted over land? What is the scheme for land processes?

R: The surface layer option is the revised MM5 Monin-Obukhov scheme, and the land-surface option is thermal diffusion scheme. Both land and sea surface temperatures are predicted, which has been included in lines 136-137.

Lines 178-179: it is stated that “The precipitation is extremely light in March and somewhat heavy in September”. This statement needs some corroborating evidence, as none of the figures shows diagnostics of precipitation intensity.

R: The hourly precipitation averaged over the whole island in each month has been calculated in Fig. 3. It shows clearly that the hourly precipitation is close to zero in both CMORPH and gauges data in March, while it becomes larger than 0.5 mm/h in September.

Line 208: as -> at?

R: “As” was revised as “representing” in line 245.

Lines 245-246, 328-330: Here surface temperature decrease is attributed to precipitation and cold pool. From the surface energy budget point of view, surface temperature is controlled by a range of processes: surface heat fluxes, both shortwave and long wave radiative processes, diffusion in the soil, etc. It is at least equally likely that decrease of surface temperature may be attributed to decreases of incoming solar heating and persistent longwave cooling.

R: Many other reasons that may have contributed to the temperature decrease have been included here. This sentence has been revised as “decreases rapidly thereafter owning primarily to the development of precipitation (which has its diurnal maximum during this period) and associated evaporative cooling. Besides, surface temperature is also controlled by other processes, such as surface heat fluxes, both shortwave and long wave radiative processes, diffusion in the soil, etc.” In Lines 367-370.

Lines 393-394: Here the discussion of cold pool may be revised since the role of diabatic heating in the whole troposphere may also be important.

R: The discussion of cold pool has been revised based on the new experiment NOVAP in lines 434-443 as “A weaker sea breeze is observed in the FakeDry experiment than in the IDEAL experiment while NOVAP experiment shows the strongest sea breeze. The NOVAP experiment generated much stronger precipitation over the island as the rain evaporation cooling process was turned off. The propagation of the LSB is much slower and the inland propagation distance is much shorter in FakeDry experiment than that in the IDEAL experiment while the propagation speed in NOVAP experiment is between the other two experiments, which suggests that cold pool can accelerate the over the tropical island. In the NOVAP experiment, the heavy precipitation does not dissipate after 2100 LST but propagates into the northeast out of the island with the land breeze, indicating that cold pool plays an important role in dissipating the convection.”

Lines 398-399: It is stated that the land sea breeze circulations “are confined to lower levels owing to weaker vertical motion”. Any evidence to support this statement of causality?

R: As the latent heating and cooling processes were turned off, the advection in FakeDry was much weakened. At the same time, the sea breeze decreased. In term of land breeze at their peak stage, the strong land breeze circulation can reach around 2 km in vertical altitude in IDEAL experiment

while it is lower than 1 km in FakeDry experiment (Fig. R1h, i vs. Fig. R2h, i). For sea breeze at their peak stage, the sea breeze circulation can extend to 5 km altitude in IDEAL experiment, while it only can reach 3 km in FakeDry experiment (Fig. R1e,f vs. Fig. R2e,f). The stronger vertical velocity (negative and positive) can extend over 5 km in IDEAL experiment, while it can only reach 2 km in FakeDry experiment. We added this evidence in the revised manuscript in Lines 448-449. Figs. R1 and R2 are the original Figs. 15 and 19. For the sake of succinctness, we removed these two figures in the revised manuscript.

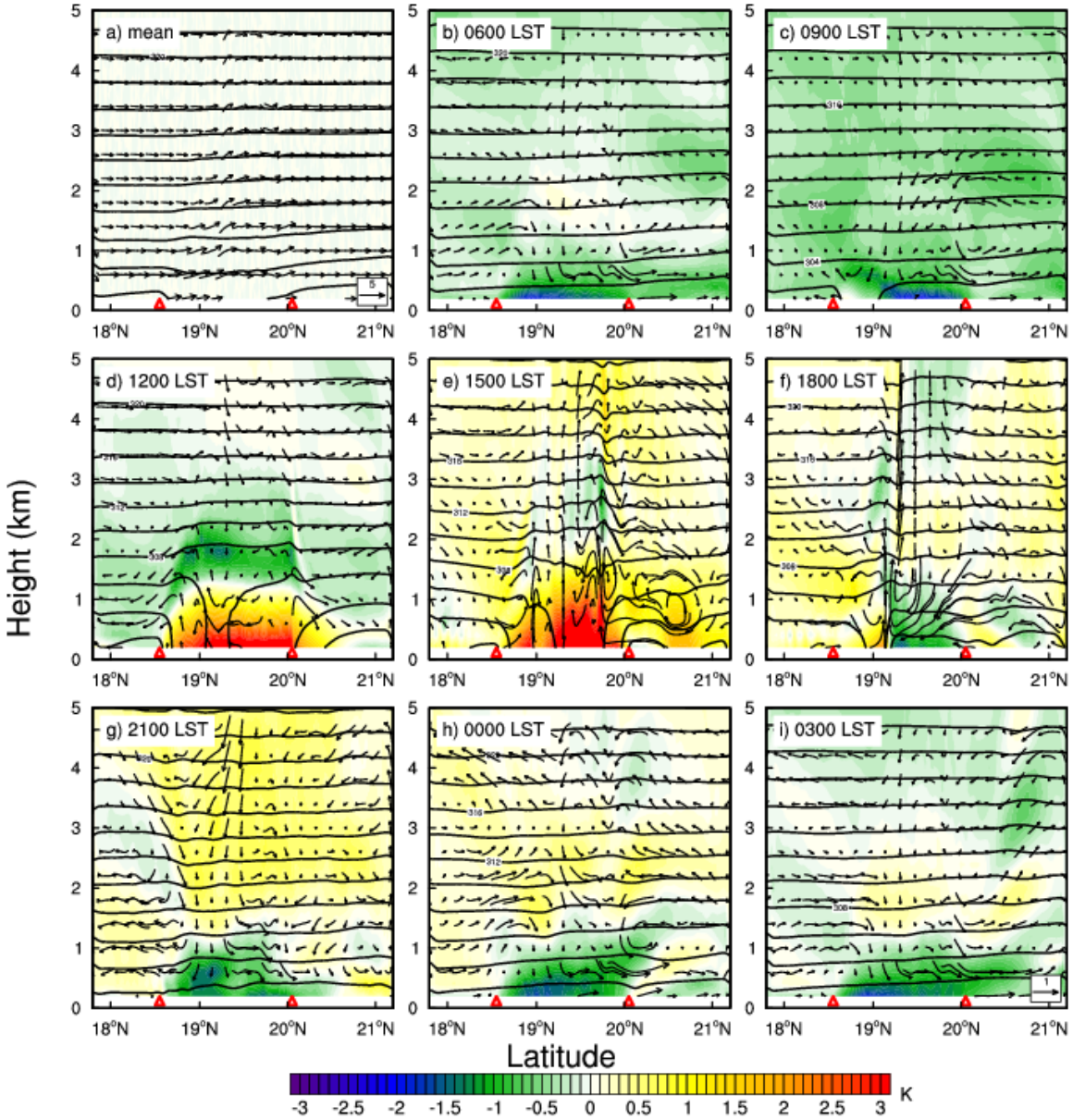

Fig. R1 Vertical cross-sections of perturbation temperature (shading), perturbation wind (vectors; the scale of the vertical component is increased by a factor of 5), and temperature (contours) in the south-to-north direction (see red line in Fig. 1) averaged over all hours (a) and at 3-h intervals (b–i) in simulation IDEAL. The triangles in each panel indicate the edges of the island.

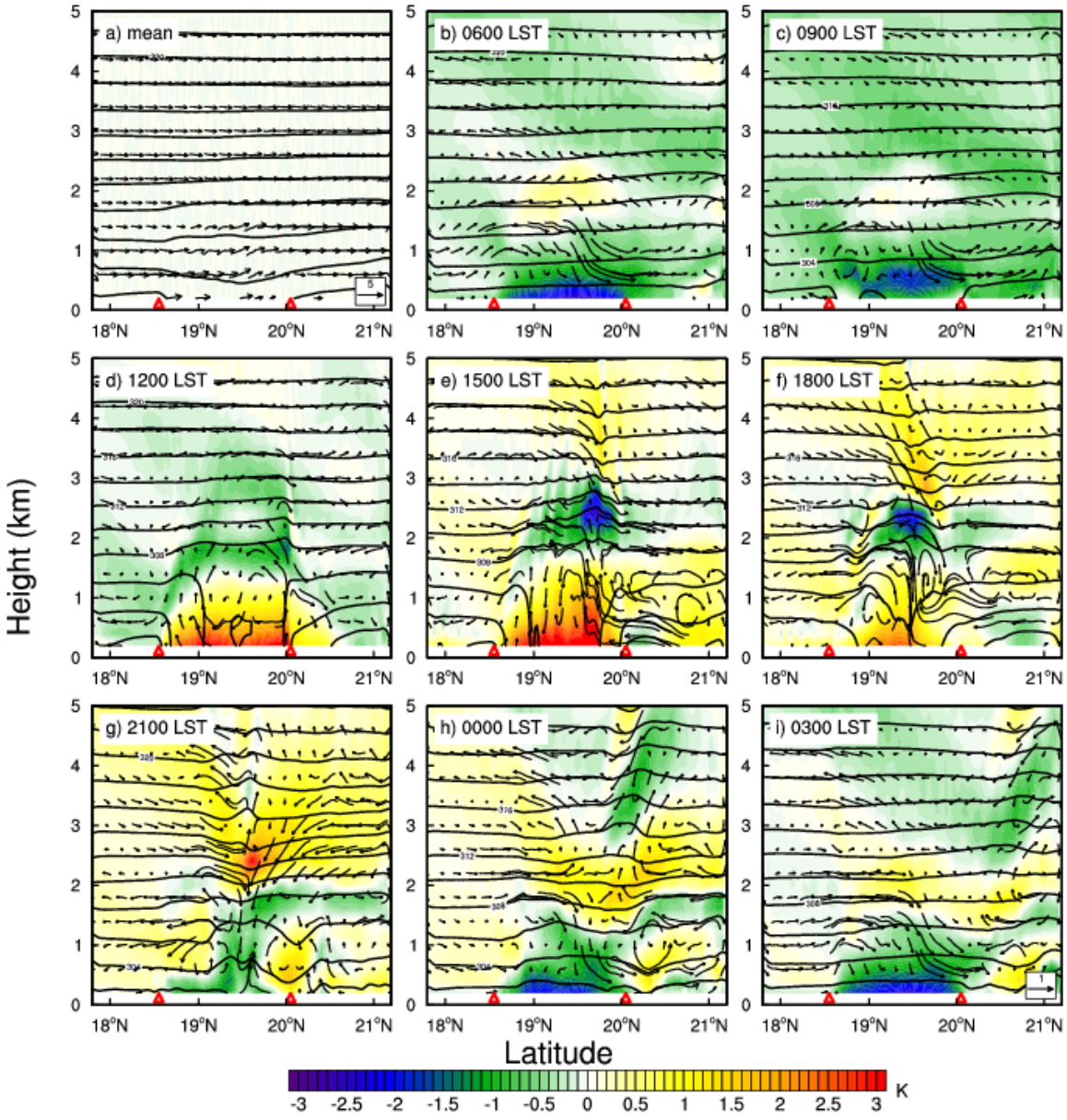

Fig. R2 Vertical cross-sections of perturbation temperature (shading), perturbation wind (vectors; the scale of the vertical component is increased by a factor of 5), and temperature (contours) in the south-to-north direction (see red line in Fig. 1) averaged over all hours (a) and at 3-h intervals (b–i) in simulation FakeDry. The triangles in each panel indicate the edges of the island.

Lines 425: Some discussion may be needed to justify using cyclic boundary conditions since none of the flow or surface boundary condition (SST) are cyclic in the horizontal.

R: Sorry for the confusion. We actually used the cyclic lateral boundary conditions rather than cyclic boundary conditions.

Lines 450-455: Model resolution may be a convenient culprit responsible for the 1-hour delay of the rainfall (which in my opinion should be not a concern). On the other hand, there can be many other factors causing this delay, for example, biases in ECMWF reanalysis data used for boundary conditions to drive the numerical simulations, biases in physical processes (microphysics, surface processes, radiative process, etc.). It is difficult to rule out these possibilities.

R: More possible reasons for the 1-hour delay have been included in the summary part in lines 518-521.

Figures 14,15,18, and 19: It makes more sense to label the horizontal axis with kilometers instead of grid points.

R: We have changed all the horizontal axis label to latitude and longitude.

The influence of sea- and land-breeze circulations on the diurnal variability of precipitation over a tropical island

Lei Zhu[1,2,3], Zhiyong Meng[1*], Fuqing Zhang[2,3], Paul M. Markowski[2]

[1]*Laboratory for Climate and Ocean-Atmosphere Studies, Department of Atmospheric and Oceanic Sciences, School of Physics, Peking University, Beijing, China*

[2]*Department of Meteorology and Atmospheric Science, The Pennsylvania State University, University Park, Pennsylvania*

[3] *Center for Advanced Data Assimilation and Predictability Techniques, The Pennsylvania State University, University Park, Pennsylvania*

Corresponding author address: Dr. Zhiyong Meng, Laboratory for Climate and Ocean–Atmosphere Studies, Department of Atmospheric and Oceanic Sciences, School of Physics, Peking University, Beijing, China.

E-mail: zymeng@pku.edu.cn

Abstract

This study examines the diurnal variation of precipitation over Hainan ~~Island~~island in the South China Sea using gauge observations from 1950 to 2010 and CMORPH satellite estimates from 2006 to 2015, as well as numerical simulations~~.~~ which is the first time to use climatological mean initial conditions and diurnally averaged periodic lateral boundary conditions to study the dynamic and thermodynamic processes (and the impacts of land-sea breeze circulations) that control the rainfall distribution and climatology. Precipitation is most significant from April to October, and exhibits a strong diurnal cycle resulting from land/sea breeze circulations. ~~-~~More than 60% of the total annual precipitation over the island is attributable to the diurnal cycle~~,~~ with a significant monthly variability as well. The CMORPH and gauge datasets agree well, except that the CMORPH data underestimates precipitation and has a 1-h delay of peaks. The diurnal cycle of the rainfall and the related land/sea breeze circulations during May and June were well captured by convection-~~allowing~~permitting numerical simulations with WRF, which were initiated from 10-year average ERA-interim reanalysis~~, despite~~ . The simulations have a slightly ~~overall~~ overestimation of rainfall amounts and a 1-h delay ~~of the rainfall~~ in peak~~.~~ rainfall time. The diurnal cycle of precipitation is ~~due to a diurnal cycle~~driven by the occurrence of moist convection~~, which initiates~~ around noontime owing to low-level convergence associated with the sea breeze ~~circulation~~circulations. The precipitation intensifies rapidly thereafter and peaks in the afternoon with the collisions of sea breeze fronts from different sides of the island. Cold pools of the convective storms contribute to the inland propagation of the sea breeze. ~~The~~Generally, precipitation dissipates quickly in the evening ~~owing~~due to the cooling and stabilization of the lower troposphere and decrease of boundary-layer moisture. Interestingly, the rather high island orography is not a dominant factor in the diurnal variation of the precipitation over the island.

37

1. Introduction

On tropical islands, the diurnal precipitation cycle tends to be driven by the land-sea breeze (LSB), as well as mountain-valley wind systems (Mapes et al. 2003; Qian 2008; Crosman and Horel 2010~~; Qian 2008; Mapes et al. 2003). ~~). Both rain gauge and satellite observations indicate that rainfall peaks in the late afternoon over inland regions, and in the early morning or evening offshore (Yang and Slingo 2001).

The emergence of high temporal and spatial resolution satellite-estimated precipitation observations, such as those provided by- Tropical Rainfall Measuring Mission (TRMM~~(~~, Huffman et al. 2007) and Climate Prediction Center Morphing Technique (CMORPH~~(~~, Joyce et al. 2004), has greatly improved our understanding of tropical precipitation. Precipitation amounts are much higher over tropical islands than their surrounding oceans (Qian 2008). More than 34% of the total precipitation in the tropics is attributable to precipitation over land (Ogrino et al. 2016). Moreover, the tropical precipitation is usually due to convection (Dai 2001), and tropical convection is well known to have an important influence on the large-scale atmospheric circulation (Neale and Slingo 2003; Sobel et al. 2011).

Many efforts have been made to understand the mechanisms behind the diurnal precipitation cycle over tropical islands. With CMORPH data and regional climate model simulation, Qian (2008) found that sea-breeze convergence, mountain-valley winds and cumulus merger process are the predominant reasons for the diurnal precipitation cycles while the underrepresentation of islands and terrain results in the precipitation underestimate. Hassim et al. (2016) examined the diurnal cycle of rainfall over New Guinea with a 4-km convection-~~allowing~~permitting WRF model. They found the importance of the sea breeze in the initiation of rainfall but focused on large-scale atmospheric properties preferential to the propagation of systems offshore at night. They also

found that orography and the coastline along with gravity waves were beneficial for the ~~diurnal cycle. Other studies have found that precipitation over tropical islands is strongly influenced by the size of the islands (Sobel et al. 2011; Cronin et al. 2014).~~longevity and maintenance of the convection systems though they are not the fundamental reasons for the convection initiation.

The diurnal cycle of tropical rainfall is usually poorly captured by most global climate models (GCMs~~),~~) and even cloud-resolving models (CRMs), owing to model uncertainties in depicting the physical mechanisms that underlie the diurnal precipitation cycle (Yang and Slingo 2001; Qian 2008; Nguyen et al. ~~2015; Hassim et al. 2016). Sometimes diurnal variability can only be~~2015). Yang and Slingo (2001) found that the deficiency of model's physical parameterizations may be the main reason for the difficulty in capturing the observed phase of diurnal cycle in convection. Diurnal variability is only captured in some places or months where the signals are strong, while at other times, the diurnal signals are captured, but with a large timing error of the maxima and minima. Studies show that the LSB may have different contributions to the diurnal variabilities of precipitation at different places (~~Yin et al. 2009; Jeong et al. 2011; Zhang et al. 2014; Zhang et al. 2016a, 2016b).~~Keenan et al. 1988; Qian 2008; Wapler and Lane 2012; Chen et al. 2017). Precipitation tends to be initiated by the convergence of land breezes (Wapler and Lane 2012) and sea breezes (Qian 2008) over gulf area and islands area, respectively. Interactions between land breeze and prevailing wind are likely to produce precipitation over the coast area or tropical islands (Keenan et al. 1988; Chen et al. 2017). Recent studies (Bao et al. 2013; Chen et al. 2016, 2017) also have found that convectively driven cold pools and latent cooling, as well as environmental wind and moisture, may play important roles in the propagation and maintenance of diurnal rainfall in coastal regions. How cold pools and latent cooling affect the diurnal cycle of rainfall and related LSB over a tropical island has not been studied extensively.

This current work is aimed at examining the diurnal cycle of precipitation and the related LSB over Hainan Island in the South China Sea. Hainan Island is a tropical island located off the southern coast of China (Fig.1). It is one of the rainiest areas in China, and is influenced by a variety of synoptic-scale and mesoscale weather systems, such as ~~a~~ monsoon, tropical cyclones, LSB, and ~~a~~ mountain-plain ~~solenoid (MPS).~~solenoids. The island's topography features mountains in the southwest, with peak ~~altitudes~~altitude of approximately 1000 ~~m~~meter above the sea level (shaded in Fig. 1), and plains in the northeast. ~~Hainan Island is the largest of the so-called "Special Economic Zones" in China. Tourism is an important part of Hainan's economy because of its beautiful beaches and lush forests. Hainan Island is frequently referred to as "Chinese Hawaii." More than nine million residents and tourists live on the island.~~

The characteristics of ~~the~~ precipitation and LSB over Hainan Island have been examined via statistical methods based on either surface observation or modeling simulations (Tu et al. 1993; Zhai et al. 1998; Zhang et al. 2014; Liang and Wang 2016). Based on nine station-based wind observations, Zhang et al. (2014) found that LSB occurs ~~rather~~more frequently in summer and autumn, though their findings are limited in using observations in only one month of one season. Most recently, Liang and Wang (2016) examined the relationship between the sea breeze and precipitation of Hainan Island using surface wind and precipitation observations along with the global reanalysis over several years. They hypothesized that the seasonal precipitation is due to the initiation of convection by the LSB, but they did not provide thorough investigation on how the LSB circulations trigger and enhance the precipitation over Hainan Island.

The objective of this study is to investigate the diurnal precipitation variation over Hainan Island and the detailed physical mechanisms related to LSB forcing and variability. This is the first time using semi-idealized convection-permitting simulations with climatological mean initial

conditions and diurnally averaged periodic lateral boundary conditions to study the dynamic and thermodynamic processes (and the impacts of land-sea breeze circulations) that control the rainfall distribution and climatology over a tropical island. We would also highlight the removal of terrain effect, along with a further simplification using a perfect oval shaped island. The study relies on rain gauge observations and satellite-derived precipitation estimates, as well as convection-~~allowing~~permitting numerical simulations. Section 2 describes the dataset and the methodology. Section 3 documents the diurnal precipitation variation in each month, as well as the percentage of the total precipitation that can be attributed to the diurnal cycle. -The relationship between the precipitation and surface winds during the first rainy season [May and June, which is defined relative to the second rainy season (July through September) of southern China when precipitation is mainly caused by typhoons] are also ~~are~~ analyzed. The model configuration and results of the simulations are presented in Section 4. Conclusions are presented in Section 5.

2. Observation dataset and methodology

Rainfall was analyzed using 19 rain gauges on Hainan Island (Fig. 1). The ~~distribution of the~~ gauges ~~is~~are relatively ~~homogeneous, and suitable for assessing~~evenly distributed across the island. The sampling frequency is one hour, which is dense enough to represent the diurnal precipitation variation over the ~~entire~~ island.- The dataset spans 60 years (1951–2010), though full records exist for only a subset of this period at some of the stations, owing to the fact that the stations were built at different times~~.~~ (the detailed dataset periods for each station are shown in Table 1). Surface temperature and wind observations obtained at the same locations over a four-year period (2007–2010) were used to investigate the land and sea breezes. The surface precipitation observations ~~were~~are augmented by National Oceanic and Atmospheric Administration (NOAA-) and Climate

Prediction Center Morphing Technique (CMORPH ~~analyses~~) data derived from low-Earth orbiting and geostationary satellites (Joyce et al. ~~2004) as shown to be valuable in past studies of diurnal precipitation over China (e.g., He and Zhang 2010; Bao et al. 2011; Sun and Zhang 2012; Bao et al. 2013; Zhang et al. 2014).~~2004). The ~~spatial and~~CMORPH grid with a temporal ~~resolutions of the CMORPH analyses are~~resolution of 30 minutes is 0.7277 degree by 0.7277 degree (approximately 8 km by 8 km~~) and 30 min, respectively. ~~). Ten years of CMORPH ~~analyses~~data (2006–2015) were used.

A series of convection-~~allowing~~permitting numerical simulations were performed with the Advanced Research Weather Research and Forecasting (~~WRF~~ARW, Skamarock et al. 2008) model version 3.7.1 to investigate dynamical features of the diurnal cycle of precipitation and its physical mechanisms~~,~~ in particular with regards to ~~the~~ LSB forcing. Initial and lateral boundary conditions were provided by the European Center for Medium-Range Weather forecast Interim (ERA-interim) reanalysis data (Dee et al. 2011) of 0.75° × 0.75° grid spacing. Only one domain was used with 225 × 205 grid points and a horizontal grid spacing of 2 km. A total of ~~53~~50 vertical levels were used with the model top at ~~10~~50 hPa. ~~The physical schemes that were used were the same as those in Chen et al. (2016), such as the~~The Yonsei University (YSU) boundary scheme (Hong et al. ~~2006) and~~ 2006), Dudhia shortwave radiation (Dudhia 1989), the Rapid Radiative Transfer Model longwave radiation scheme (Iacono et al. 2008), the single-moment 5-class microphysics ~~scheme~~ (Hong et al. 2004), ~~except that~~five-layer thermal diffusion land surface and Revised MM5 surface layer schemes were used, while no cumulus parameterization was used in this study.

The initial conditions of all simulations were the average of ERA-interim reanalysis data at 0000 UTC in May and June of 2006–2015. The lateral boundary conditions were obtained in the same way as the initial conditions, cycled from 0000 to 0600, 1200, 1800 and 0000 UTC.

Experiment REAL was initiated with the unmodified initial and lateral boundary conditions to simulate the diurnal characteristics. Experiment NoTER is the same as REAL except that the orography over Hainan Island is removed in the initial conditions in order to isolate the influence of the island's terrain. Simplifying the influences of land category and coastline, experiment IDEAL was constructed with an idealized elliptical island to replace the real Hainan Island in the initial condition. The idealized island has a similar size and orientation, and is located at the same place as Hainan Island (Fig. 1), covered with uniform grassland (LU_INDEX=7 in WRF model) while other areas of the model domain are set as ocean. In order to examine the impact of latent heating/cooling on the LSB and related rainfall, sensitivity experiment FakeDry was performed similar to the IDEAL experiment, except for turning off latent heating and cooling in the model (no_mp_heating=1 in WRF model). Another sensitivity experiment NOVAP was performed similar to IDEAL experiment except for turning off the evaporation of liquid water, which prevents the cold pool generation from moisture convection process. A similar methodology has been used to study diurnal cycle of precipitation in many different regions (Trier et al. 2010; Sun and Zhang 2012; Bao and Zhang 2013; Chen et al. 2016, 2017). The biggest advantage of this method is that it is able to capture the general characteristics of the diurnal cycle of precipitation and the related dynamical processes instead of just focusing on a single case. All simulations were integrated for one month. The mean over the last 26 days was used for the analyses in order to alleviate the spin-up issue and day-to-day variability.

3. Observation analysis

3.1. Diurnal variation of precipitation and its seasonal-dependent features

Diurnal variations of precipitation were examined at each single station in each month based on the hourly gauge precipitation observation averaged over the period from 1951 to 2010. The hourly precipitation evolution shows a significant seasonal cycle over the island. Most of the precipitation falls from April to October, which is the monsoon season, and exhibits a distinct diurnal cycle during that period, whereas less precipitation and lack of a strong diurnal cycle characterize the other months (Fig. 2). -The seasonal variability is related to the annual cycle of the East Asian Monsoon. April and September are the two transitional periods of the low-level prevailing wind; the prevailing wind strongly influences the transport of water vapor and precipitation.

The diurnal precipitation cycle has ~~its~~the maximum precipitation at 1500 local standard time (LST, LST=UTC+8) in most months during the warm season, except at 1600 LST in April and July. No second precipitation peak is observed, which is different from studies of other tropical islands in which a second peak between midnight and early morning has been noted (Kishtawal and Krishnamurti 2001; Wapler and Lane 2012~~; Chen et al. 2016).~~). The second nocturnal peak was found to be closely related to convection caused by ~~the MPS~~mountain-plains solenoid that propagates offshore and coincides with the land breeze during the night or early morning.

The diurnal precipitation cycle shows location-dependent features (Fig. 2). ~~No distinct~~ We grouped the stations with different colors based on their similarity in diurnal variations which to a large extent are correlated with their geographical locations. No heavy rainfall or distinct variability ~~of rainfall~~ is observed at stations ~~denoted by blue lines. These stations, denoted by blue dots in Fig.1, are located~~ along the southern coastline ~~where there is no heavy~~ (blue dots on Fig. 1 and ~~diurnal precipitation.~~blue lines on Fig. 2). All the rest of the island stations share similar diurnal peak precipitation times with the red-dot stations (in red lines) having the highest peak

values from April to July~~,~~ while in August and September both the red-dot and black-dot stations (mostly inland) share ~~the~~ strongest peaks.

Even though the distribution of gauge-based precipitation ~~stations~~station is ~~rather homogeneous~~relatively even across the island, the observations are still too sparse to analyze the detailed rainfall pattern ~~in detail~~ over the island. For this reason, satellite-derived precipitation CMORPH data were also ~~are~~ used to examine the diurnal rainfall variation for each of the 19 gauge stations. The hourly diurnal precipitation variation derived from the CMORPH ~~analyses~~data agrees well with the rain gauge observations in each month (Fig. 3), though the CMORPH amounts are slightly smaller. The time of peak precipitation in the warm season (from May to August) is delayed by one hour in most months in the CMORPH ~~analyses~~data (maximum at 1600 LST) relative to the peak in the gauge-based observations. These results indicate ~~that~~good agreement between the CMORPH data ~~are able to expose the diurnal precipitation cycle over this tropical island well in comparison with the~~and gauges, in particular for the warm-season months that are the focus of this study.

The percentage of the diurnal precipitation ~~(DP)~~ in the total precipitation over the island in each month was examined with the CMORPH data (Fig. 4). Similar to He and Zhang (2010) and Bao et al. (2011), the diurnal precipitation percentage was defined as the mean rainfall rate at each 1-hour interval by ~~DP $=\frac{\sum_{t=0}^{23}|(r_t-\bar{r})|}{r_d}$~~, diurnal precipitation percentage $=\frac{\sum_{t=0}^{23}|(r_t-\bar{r})|}{r_d}$, in which, r_t is the mean hourly precipitation at each hour t (0–23), $\bar{r}$ is the mean hourly precipitation at all hours, and the r_d is the daily mean precipitation. The diurnal precipitation percentage represents a large percentage of the total precipitation over the island in most months (Fig. 4). In particular, the total precipitation in May is almost entirely attributable to the diurnal cycle (Fig. 4e). The diurnal contribution of the total precipitation exceeds 60% averaged for the whole year and over the whole

island, although the magnitude is smaller in September and October. The diurnal precipitation percentage value exceeds 20% in August and September (Figs. 4h and i). Moreover, the area exhibiting a large magnitude of diurnal precipitation roughly coincides with the region also having the most accumulated precipitation. However, the diurnal precipitation percentage is not quite related to the precipitation intensity. The precipitation is extremely light in March and somewhat heavy in September. ~~-~~However, the diurnal precipitation percentages are reversed (~~lesser~~smaller percentages in September, ~~higher~~greater percentages in March), which is likely related to different physical processes of the precipitation in those months. The detailed physical processes that lead to the steady decrease of diurnal precipitation percentage from May to October before increasing again are beyond the scope of the current study. The possible reasons could be attributed to the synoptic scale storms, typhoons, prevailing winds, the land sea temperature contrast and atmospheric moisture content, which will be explored in our future study.

3.2. The diurnal cycle of precipitation, land breezes, and sea breezes in May and June

A more detailed analysis of the diurnal rainfall variation in May and June was carried out because of the intense hourly mean rainfall and high ~~DP~~diurnal precipitation percentage. In May, the prevailing warm and wet southwest monsoon airflow transports abundant moisture from the ocean to Hainan Island. A distinct diurnal cycle of precipitation, with a single peak between 1200 and 2000 LST, is evident in both the gauge-based and CMORPH data (Fig. 5). The datasets agree well with each other at each surface station, except that ~~the~~ CMORPH data exhibit larger peak values at the red and green stations. Four gauge-based stations in blue have a much weaker daytime peak. These stations, however, have an apparent nocturnal peak, whereas other stations do not exhibit a nocturnal peak. The nocturnal precipitation is possibly attributable to the convergence

between the low-level prevailing wind and ~~MPS~~downhill jet circulations, which are to be examined with the numerical simulations in section 4. The average over all stations (thick black line in Fig. 5) also exhibits an obvious diurnal cycle.

The horizontal distribution of precipitation was analyzed using the CMORPH data (every 3 h ~~in Fig.~~except for using 1700 LST as it is the strongest rainfall time in CMORPH data in Fig. 6) along with the perturbation surface wind at gauge stations, which was obtained by subtracting the daily mean from the total wind to highlight the diurnal cycle. The precipitation averaged over all times shows that the precipitation mainly appears in the northeast in the lee-side of mountainous area (Fig. 6a). The gauge-based stations with significant diurnal cycle (in red dots) are located over the heaviest rainfall region while the gauge-based stations with non-distinctive diurnal feature (in blue dots) are located in the weakest precipitation area. Hourly variation of precipitation shows that there is little precipitation over the island in the early to mid-morning (0000 to 0900 LST), which is on average less than that over the surrounding ocean. At 0600 LST, the perturbation surface wind at gauge stations has an offshore direction in coastal area, a signature of nighttime land breeze (Fig. 6b). Three hours later at 0900 LST, the perturbation wind strengthens and turns to the right of its previous direction, particularly along the coast (Fig. 6c). At 1200 LST, the wind has changed to onshore direction ~~as~~representing the beginning of sea breeze, along with the start of weak inland precipitation where the sea breeze converges (Fig. 6d). In the next several hours (Figs. 6e–f), the rainfall intensifies rapidly, reaching to the peak at around 1700 LST. The heaviest precipitation concentrates in the northeast island corresponding to strong convergence of sea breeze (Fig. 6f). The precipitation dissipates rapidly thereafter and there is almost no precipitation by 0300 LST (Figs. 6g–i). The perturbation wind also weakens quickly and turns to offshore along the northern coast. The magnitude of the perturbation wind is close to zero over the island at 2100

LST (Fig. 6g). The land breeze intensifies slowly and nocturnal precipitation initiates along the southeast coast of the island (Fig. 6h). The nocturnal precipitation intensifies to the peak and expands to a larger area at 0300 LST, ~~whereas~~while the precipitation decreases to a minimum (near zero) over the central island (Fig. 6i).

Although the analyses on the precipitation and surface wind observation can efficiently reflect general features of the diurnal rainfall variation and the LSB, they cannot be used to examine the detailed dynamics and thermodynamics processes of the diurnal precipitation cycle and the related LSB over the tropical island. The three-dimensional structures of the LSB, as well as the mechanism of how the LSB triggers and enhances the diurnal precipitation cannot be resolved by the surface observation alone. These aspects were examined using a numerical model, as discussed in the next ~~session~~section.

4. Numerical ~~simulations~~simulation results

~~As described in the methodology section, all numerical simulations were initiated at 0000 UTC with the same diurnally cycled boundary conditions, both derived from a 10-year climatological mean represented by the ERA-interim reanalysis for May and June during 2006–2015. The initial conditions were modified for different purposes. Experiment REAL was initiated with the unmodified initial conditions. Experiment NoTER is the same as REAL, except that the orography over Hainan Island is removed in the initial conditions in order to isolate the influence of the island's terrain.~~

4.1. The simulated diurnal cycle and the influence of the orography

The REAL simulation reproduces the diurnal cycle of precipitation and the associated LSB. The diurnal variations of the 2-meter temperature, 2-meter temperature tendency, and precipitation averaged over the last 26 ~~days~~day of the WRF simulations ~~at~~and all stations over the island (Fig. 7) show generally good agreement with the observations except for slightly higher peak values of simulated 2-meter temperature and ~~greater~~ simulated precipitation (cf. Figs. 7a and 7b). The overall process of the diurnal variation over the island was well simulated, suggesting that the ~~adopted numerical model have~~chosen setup of WRF-ARW has the ability to capture the radiative effect due to solar insolation well. The surface temperature begins to increase at 0600 LST and peaks at 1300 LST, coincident with the increase of solar heating. With the rainfall evaporation cooling rate becoming larger than the solar heating rate and/or the radiative cooling later on, the temperature starts to decrease thereafter. After sunset, the temperature drops continuously, reaching its minimum near 0600 LST.

The horizontal distribution of precipitation averaged in REAL (Fig. 8a) also has reasonably good agreement with that of the CMORPH data at all hours (Fig. 6a), although the simulated precipitation is slightly larger. The area of heavy precipitation at the center of the island is well captured by the WRF simulation, although the magnitude is noticeably overestimated. The diurnal precipitation cycle is also well revealed by the variation in the horizontal distribution of the simulated precipitation although with a slightly larger magnitude and a 1-hour delay in peak time. The evolution of the simulated surface perturbation wind (on the second lowest model level for horizontal wind, which is the 0.994-sigma level, about 50 meters above the surface) is also consistent with the observation despite some discrepancy in magnitude (Figs. 6 and 8), suggesting that the LSB is well captured as well. However, the evening rainfall along the southern coast is missing, which is likely because the resolution we used in this study was still too coarse to resolve

the convection over the southern coast or the physical process was so complex that the model is unable to represent it for now.

The results of the NoTER simulation (with removal of island orography) are highly consistent with those of REAL in terms of both the magnitude and timing of each variable averaged over the whole analysis period and at all stations (Figs. 7b and c). Similar results are also found in the horizontal distribution features (~~Figs~~Fig. 8 and Fig. 9). Neither the pattern nor the magnitude is altered meaningfully between the two simulations. These results suggest that the diurnal cycle characteristics are not sensitive to the orography over Hainan Island, although many previous studies demonstrated that the orography can play an important role in the precipitation over other islands (Sobel et al. 2011; Hassim et al. ~~2016~~2016; Barthlott and Kirshbaum 2013).

In order to simplify the influences of land category and coastline, experiment IDEAL was ~~further~~ constructed with an idealized elliptical island to replace the real Hainan Island in the initial condition. ~~The idealized island has a similar size and orientation, and is located at the same place as Hainan Island (Fig. 1), covered with uniform grassland while other areas of the model domain are set as ocean.~~ The diurnal variation of the 2-meter temperature (blue), 2-meter temperature tendency (red) and hourly accumulated precipitation (green) in IDEAL (Fig. 7d) are nearly identical to those in REAL (Fig. 7b) and the station observation (Fig. 7a) except for their larger magnitudes which could be related to the modified surface land category and the smoothed ellipsoidal coastlines. The diurnal variations of the hourly accumulated precipitation and perturbation wind on the second lowest model level for horizontal wind (Fig. 10) in IDEAL simulation show that the timing of the LSB transitions and the precipitation location are quite similar to those in REAL and the observation with much smoother distribution in the horizontal perturbation wind and precipitation over the island. The relationship between the diurnal variation

of precipitation and LSB will be further examined in details based on the results of IDEAL in the next section.

4.2. Diurnal variation of precipitation and the related LSB in IDEAL

The mean fields ~~for~~ averaged over all hourly model output times during the last 26 days of the simulation depict a southerly low-level prevailing flow over the whole domain, which transports warm moist air to the island from the South China Sea (Fig. 10a). Greater moisture appears in the northern island over the heavy precipitation area under the influence of southwesterly low-to-mid-level flow (850 hPa, Fig. 11a). Higher surface temperature appears over the southern side than that in the northern side (Fig. 12a).

Based on the different phases of surface temperature and perturbation wind, we divided the diurnal cycle process into four stages to elucidate the mechanisms in each stage. The four stages are ~~the~~ establishment of a sea breeze (0600–1200 LST), peak sea breeze and peak precipitation (1200–1800 LST), establishment of a land breeze (1800–0000 LST), and peak land breeze phase (0000–0600 LST), respectively. More detailed analyses will be focused on the two middle stages. These are ~~the~~ most complicated stages, but are also the most pertinent to the heavy diurnal precipitation (and are therefore most interesting).

a. Stage 1. Establishment of a sea breeze (0600–1200 LST)

This stage commences with the onset of surface heating following sunrise. Because ocean and land have different heat capacities, the island is heated faster than the surrounding ocean. The temperature gradient between the island and the surrounding ocean gradually reverses from

offshore to onshore, which results in the weakening and demise of land breeze, and the establishment of a sea breeze over the island.

In ~~the~~ early morning hours when the sun is just about to rise, surface air temperatures over the island attain their lowest readings, with air temperatures being a few degrees lower than over the surrounding ocean (Fig. 12b). Owing to persistent solar heating, the surface air temperature over most part of the island exceeds ~~that over~~ the ocean by 0900 LST (Fig. 12c). Meanwhile, the surface air temperature gradient is directed from offshore to onshore, although the land breeze still persists over the island at this time.

The local rate of warming is inhomogeneous over the island. ~~Surface temperatures~~The surface temperature in the northeastern part of the island are considerably lower than that in other regions where the temperatures surpass the surrounding ocean by 0900 LST. The slower warming in the northeastern part of the Hainan Island is likely due to the morning fog or cold pool air (Fig. 13b) that commonly forms ~~overnight~~ within the area humidified (Fig. 14b) by late-afternoon precipitation on the preceding day ~~(Fig. 14b).~~. The ~~fog~~cloud over the area attenuates solar radiation and subsequently slows the local warming. Moreover, positive horizontal temperature advection exists over the southern island (Fig. 15a and b), which helps to increase the temperature faster over the area. The sea breeze begins to develop along the southwestern coastline owing to the weakest land breeze and the highest warming rate, while other areas of the island are still under the control of the land breeze with an offshore temperature gradient (Fig. 12c). Two land- breeze circulations (LBCs) appear clearly in the vertical direction below 3 km along the coast of the island at 0600 LST (Fig. ~~15b~~14b). The southern LBC recedes quickly with the reversal of the temperature gradient at around 0900 LST, while the other LBC remains distinct (Fig. ~~15c~~14c).

By 1200 LST, the temperature gradient reverses to the onshore direction, while the sea breeze has fully established along the entire coastal line (Fig. 12d). Unevenly warming speeds over the island with much more rapid warming over the north while slower warming over the south, which is a result of a high negative horizontal temperature advection over the southern island along the coastlines (Fig. 15d). A sea-breeze front appears at the leading edge of the sea breeze along the coastline, particularly along the northernmost coast where the maximum near-surface temperature gradient lies (Fig. 12d). At the same time, copious water vapor is transported inland from the ocean owing to the low-to-~~midlevel~~mid level prevailing wind (Fig. 11d) and upward motions (Fig. 14d). Clouds initially form along the sea-breeze ~~front (Fig. 13c) and subsequently produce rainfall (Fig. 10d~~(Fig. 13c) and subsequently produces rainfall (shaded in Fig. 10d and green lines in Fig. 13d). Noticeably, more rapid warming during this period happens over the northwest of the island while it is much slower over the other areas (Fig. 12d), which is because of the horizontal gradient and advection of the temperature over the whole island (Fig. 15).

b. Stage 2. Peak sea breeze and peak precipitation (1200–1800 LST)

Surface temperature is a maximum from 1200 to 1400 LST over most of the island, then decreases rapidly thereafter ~~owing~~owning primarily to the development of precipitation (which has its diurnal maximum during this period) and associated evaporative cooling. Besides, surface temperature is also controlled by other processes, such as surface heat fluxes, both shortwave and long wave radiative processes, diffusion in the soil, etc. The sea breeze also reaches its peak ~~intensity~~intensify in the 1200–-1400 LST time period.

At 1500 LST, surface temperature decreases over the rainfall area owing to ~~evaporative~~evaporation cooling~~,~~ and slightly increases over other areas because of continuous

solar heating (Fig. 12e). There is significant enhancement in upward motions in the low to middle troposphere (Fig. ~~15e~~14e). The sea breeze reaches its peak strength and greatest inland penetration (Fig. 12e). Two distinct sea breeze circulations (SBCs) are clearly seen in the vertical cross section, with the stronger one over the northern flank of the island (Fig. ~~15e~~14e). Moisture air is transported from ocean to the ~~northern part of the~~ island persistently by the deep southwesterly prevailing wind throughout the lower troposphere (Fig. 11e~~). At the same time, enhanced vertical motions transport the~~) while low-level convergence of moisture ~~to~~ air generating strong updraughts, which results in an increase of the moisture over the midlevels (Fig.14e). ~~-~~These factors favor the development of deep convection over the northern flank of the island ~~(Fig. 13e).~~ . As a result, precipitation increases significantly along the sea breeze front (Fig. 10e).

By 1800 LST, the strongest rainfall falls over the island (Fig. 10f) owning to strongest low-level convergence and subsequent lifting of warm moist air (Fig. 14f). The sea breeze fronts move further inland and collide with each other near the center of the island (Fig. 12f), with a deep layer of moisture over the northern side of the island that fuels the strong precipitation (Figs. 11f and 14f). Cold pools form due to the ~~evaporative~~evaporation cooling of the precipitation, contributing to the ~~formation~~propagation and ~~organization~~enhancement of ~~new convection, which further adds to~~ the precipitation, which will be further examined with two other sensitivity experiments in the next part. The precipitation pattern (Fig. 10f) exhibits a horseshoe shape aligned with the prevailing wind direction, which is similar to the result of the urban heat island study by Han and Baik (2008).

c. Stage 3. Establishment of a land breeze (1800–0000 LST)

During this period, the convection quickly dissipates and the sea breeze is replaced by a land breeze (Figs. 10g and h) after sunset. The surface temperature decreases continuously throughout

this stage over the island. The rate of temperature decrease is fastest in the first several hours ~~(Fig.,~~ reaching around -1.5 K h^{-1} at 1800-1900 LST (red line in Fig. 7d) due to the sudden loss of solar heating. The horizontal temperature gradient begins to reverse, which eventually leads to the establishment of the land breeze (Figs. 12g and h). By 2100 LST, approximately two hours after sunset, temperature over the island is decreasing rapidly both at the surface (Fig. 12g) and throughout the boundary layer ~~(Fig. 15g).~~. Meanwhile, subsidence becomes dominant over the island (Fig. ~~15g~~14g). The subsidence dries the lower levels and rainfall has ceased over the whole island (Fig. ~~14g~~13g).

By 0000 LST, with the continuous decreasing of temperature and amplifying of the offshore temperature gradient, the land breeze circulations are well established in particular across the shore of the northern island (Fig. ~~15h~~14h). Further drying is seen in mid-to-low levels as the much stronger downward flow occurs over the island, which transports dry air from aloft to the mid-to-low levels (Figs. 11h and 14h). At the same time, under the influence of the prevailing wind, much more moisture air is concentrated over the northern island, so the moisture over the northern island is much moister than the southern island. Clouds vanish quickly and precipitation dissipates almost completely by this time ~~(Fig. 13h).~~.

d. Stage 4. Peak land breeze (0000–0600 LST)

The land breeze reaches its maximum intensity during this period. Nighttime radiative cooling results in the minimum temperature being attained at approximately 0500 LST. From 0000 to 0300 LST, the land breeze intensifies rapidly along the northwest coast, becoming nearly perpendicular to the coastline and parallel with the low-level prevailing wind as the surface temperature over land decreases (Fig. 12i). Two LBCs are evident in the vertical cross section (Fig. ~~15i~~13i).

Subsidence extends over the entire island (Fig. 14i). The peak land breeze is established at 0600 LST ~~-~~(Fig. 12b). The strong subsidence also leads to further midlevel drying (Fig. 11b). Near the surface, the cooling is associated with an increase in the relative humidity, which ~~leads to~~induces the formation of low clouds and fog (~~Figs~~Fig. 13b~~ and 14b~~).

4.3. The impacts of latent heating/cooling on ~~the~~ LSB and the related rainfall

~~In order to examine the impact of latent heating/cooling on the LSB and related rainfall, a "FakeDry" simulation was performed similar to the IDEAL experiment, except for turning off latent heating and cooling in the model.~~ Surface temperature in the FakeDry experiment agrees well with the IDEAL over the island ~~(cf. Figs. 12 and 16),~~, which indicates that the solar heating rather than the latent heating/cooling is primarily responsible for the temperature variability. Although the precipitation is decreased significantly ~~(cf. Figs. 10 and 17),~~ light rainfall still occurs in the late afternoon in conjunction with the sea breeze front, but with an approximate 3-h delay in ~~convection~~convective initiation. The precipitation attains its maximum at 1800 LST, which along with the peak sea breeze, also lags that in the IDEAL experiment by approximately three hours ~~(cf. Figs. 10e and 17f).~~.

The impact of cold pool and latent cooling on the sea breeze and rainfall was further examined using the Hovmöller diagrams of zonal wind ~~perturbation~~perturbations on the second lowest model level for horizontal wind and hourly precipitation along the red line in Fig. 1 for ~~both~~ experiments IDEAL ~~and~~, FakeDry and NOVAP (Fig. ~~18~~16). A weaker sea breeze is observed in the FakeDry experiment than in the IDEAL experiment~~.~~ while NOVAP experiment shows the strongest sea breeze. The NOVAP experiment generated much stronger precipitation over the island as the rain evaporation cooling process was turned off. The propagation of the LSB is much slower and the

inland propagation distance is much shorter in FakeDry experiment than that in the IDEAL experiment while the propagation speed in NOVAP experiment is between the other two experiments, which suggests that ~~the~~ cold pool can accelerate the ~~propagation and intensification of the sea breeze~~precipitation over the tropical island. In the NOVAP experiment, the heavy precipitation does not dissipate after 2100 LST but propagates into the northeast out of the island with the land breeze, indicating that cold pool plays an important role in dissipating the convection. Moreover, given precipitation varies precisely with the convergence and divergence of horizontal winds due to LSB in ~~both~~all simulations, it is evident that the LSB is the primarily forcing for the diurnal precipitation variability over the island.

The LSB circulations in the FakeDry experiment are similar to those in the IDEAL experiment, even consistent with NOVAP experiment, except that they are confined to lower levels (around 2 km) owing to weaker vertical motion (~~Fig. 19).~~Strong vertical velocity can extend over 5 km in IDEAL experiment, while it can only reach 2 km in FakeDry experiment. Figures omitted). The latent heating can strengthen vertical ~~motions~~movement and extend the LSB circulations to higher altitudes. The latent heating feedback can also lead to stronger and earlier convection initiation and precipitation along the sea- breeze fronts. In turn, the cold pool further promotes the inland penetration of the sea-breeze front and ~~enhances the precipitation (cf. Figs. 18a and 18b).~~ dissipates the precipitation (Fig. 16), which is because the pressure gradient increases and drives the sea breeze flow more inland when cold pool moves toward the island/inland.

5. Summary

Diurnal cycle of precipitation over tropical area is poorly captured by numerical models, owing to model uncertainties in depicting the physical mechanisms that underlie the diurnal

precipitation cycle, which is considered to be closely linked with the land-sea breeze. This study explored the diurnal precipitation variation and its relationship with the land/sea breeze circulations on Hainan Island, a tropical island located off the southern coast of China, based on gauge observation and satellite-estimated precipitation, as well as convection-~~allowing~~permitting numerical simulations. The diurnal cycle of precipitation in each month over the island was analyzed with 19 gauge observations during 1951–2010. Most precipitation ~~fell~~fall during ~~the~~ warm season (from April to October) and ~~exhibited~~exhibit a significant diurnal cycle, whereas much lesser precipitation ~~fell~~fall in other months. Precipitation is a maximum between 1500–1700 LST in the warm season at almost all stations except for four stations along the southern coastline of the island.

The satellite-derived CMORPH precipitation estimates from 2006–2015 were further used to validate the diurnal precipitation variation. The CMORPH data agrees well with gauge ~~observations~~observation except for a smaller magnitude of precipitation and a 1-hour delay in the timing of the daily precipitation maximum during the warm season. The analyses on CMORPH data ~~analyses~~ show that about 60% of the total annual precipitation over the island is attributable to diurnal variations, with the largest proportion in May and the smallest proportion in September and October. For May and June, precipitation begins around local noon time, intensifying quickly thereafter, and reaching a peak at ~1500 LST based on station observations. This diurnal rainfall cycle is, for the most part~~,~~ consistent with the diurnally varying low-level wind convergence and divergence.

A series of numerical simulations (REAL, NoTER, IDEAL, FakeDry and NOVAP) using a convection-~~allowing~~permitting configuration of the WRF model (2-km horizontal grid spacing) were conducted to understand the underlying mechanisms of the diurnal precipitation variations.

The initial and cyclic lateral boundary conditions were generated using a 10-year (2006–2015) average of ERA-interim data for May and June. ~~It is found~~Results show that the orography of Hainan Island may be of only secondary influence on the diurnal precipitation cycle, which is different from past studies on other hilly islands. Similar diurnal cycles of precipitation and related land/sea breeze circulations were simulated between simulations with and without orography over the island. Even with an idealized island, which is an elliptical flat island located at the same place with similar area and orientation, but only grassland land cover, the diurnal cycle characteristics can still be fairly well captured. Those results show that: (1) WRF is capable of replicating the important aspects of the mean diurnal cycle compared to rainfall observations, (2) removing the orography and coastal features made little difference to the diurnal cycle during the rainiest times of the year, (3) the dominant process that produces the diurnal cycle were shown to be the sea/land breezes caused by the relative surface heating/cooling of the island compared to the surrounding ocean, and (4) evaporative cooling as part of convective systems also plays an important role in the diurnal cycle.

The simulated diurnal cycle of precipitation and related land/sea breeze circulations based on the idealized flat-island simulation were divided into four stages in terms of the evolutions of temperature, winds and precipitation. Stage 1 is from 0600 to 1200 LST, during which time the land breeze is replaced by a sea breeze as solar heating warms the interior of the island. Abundant moisture is transported to the low to middle troposphere over the island, resulting in ~~convection~~convective initiation and precipitation along the sea-breeze front. Stage 2 is from 1200 to 1800 LST, during which time sea breeze attains to its peak intensity and precipitation is a maximum. The sea breezes from opposite sides of the island eventually penetrate all the way to the island's center and collide, which results in the maximum precipitation being located there.

Stage 3 is from 1800 to 0000 LST, during which time a land breeze is established as a result ~~of~~the cooling over the island.~~–~~ The cooling is due primarily to the sudden loss of solar heating. Subsidence from the land breeze prevents further precipitation by early evening. The last stage covers the peak of the land breeze, which is observed near sunrise.

The FakeDry ~~experiment shows~~and NOVAP experiments show that the latent cooling and cold pool have a small impact on the land/sea breeze circulations but can apparently enhance precipitation. Strong convection can enhance the sea breeze, and the augmentation of the sea breeze by the evaporatively driven cold pool helps to accelerate the inland propagation of the sea breeze~~.~~ and weakens the convection.

Finally, it is worth mentioning that the 1-hour delay in the timing of the maximum precipitation in the simulation is probably caused by the 2-km horizontal resolution, which may not be high enough to resolve explicit underlying physical ~~process~~processes. It is likely for the same reason that the weak nocturnal precipitation is not captured by the simulations. Much higher horizontal and vertical resolution might be needed in the future work to resolve more detailed processes related to the diurnal ~~rainfall cycles~~cycles. On the other hand, there are many other factors like biases in ERA-Interim reanalysis data used for the initial and boundary conditions to drive the numerical simulations and biases in physical processes (microphysics, surface processes, radiative process, etc), which will be studied in follow-on work. Moreover, the rainfall for different seasons shows quite different patterns, owing to various underlying dynamic and thermodynamic physics. In addition to May and June that were mainly examined in this current work, the diurnal rainfall variation in other months needs to be explored in further studies.

562 **Acknowledgments:** Lei Zhu is supported by the Natural Science Foundation of China Grant
563 41461164006, and the Chinese Scholarship Council (CSC). Zhiyong Meng is supported by the
564 Natural Science Foundation of China Grants 41461164006, 41425018 and 41375048. Fuqing
565 Zhang is supported by the Office of Naval Research Grant N000140910526 and the National
566 Science Foundation Grant AGS-1305798. Paul Markowski is supported by National Science
567 Foundation grant AGS-1536460 and National Oceanic and Atmospheric Administration awards
568 NA15NWS4680012 and NA14NWS4680015. The simulations were performed on the Stampede
569 supercomputer of the Texas Advanced Computing Center (TACC). All data are freely available
570 from sources indicated in the text or from the corresponding author upon request (Email:
571 zymeng@pku.edu.cn).

References

Bao, X., Zhang, F. and Sun, J., 2011. Diurnal variations of warm-season precipitation east of the Tibetan Plateau over China. *Monthly Weather Review*, *139*(9), pp.2790–2810.

Bao, X. and Zhang, F., 2013. Impacts of the mountain-plains solenoid and cold pool dynamics on the diurnal variation of warm-season precipitation over northern China. *Atmos. Chem. Phys*, *13*, pp.6965–6982.

Barthlott, C., and D. J. Kirshbaum, 2013: Sensitivity of deep convection to terrain forcing over Mediterranean islands. *Q. J. R. Meteorol. Soc*., *139*, pp.1762–1779.

Chen, X., Zhang, F. and Zhao, K., 2016. Diurnal Variations of the Land–Sea Breeze and Its Related Precipitation over South China. *Journal of the Atmospheric Sciences*, *73*(12), pp.4793–4815.

Chen, X., Zhang, F. and Zhao, K., 2017. Influence of Monsoonal Wind Speed and Moisture Content on Intensity and Diurnal Variations of the Mei-yu Season Coastal Rainfall over South China. *Journal of the Atmospheric Sciences*, *in review*.

~~Cronin, T.W., Emanuel, K.A. and Molnar, P., 2015. Island precipitation enhancement and the diurnal cycle in radiative-convective equilibrium. *Quarterly Journal of the Royal Meteorological Society*, *141*(689), pp.1017–1034.~~

Crosman, E.T. and Horel, J.D., 2010. Sea and lake breezes: a review of numerical studies. *Boundary-layer meteorology*, *137*(1), pp.1–29.

Dai, A., 2001. Global precipitation and thunderstorm frequencies. Part I: Seasonal and interannual variations. *Journal of climate*, *14*(6), pp.1092-1111.

Dee, D.P., Uppala, S.M., Simmons, A.J., Berrisford, P., Poli, P., Kobayashi, S., Andrae, U., Balmaseda, M.A., Balsamo, G., Bauer, P. and Bechtold, P., 2011. The ERA-Interim reanalysis: Configuration and performance of the data assimilation system. *Quarterly Journal of the royal meteorological society*, *137*(656), pp.553–597.

Dudhia, J., 1989. Numerical study of convection observed during the winter monsoon experiment using a mesoscale two-dimensional model. *Journal of the Atmospheric Sciences*, *46*(20), pp.3077-3107.

Han, J.Y. and Baik, J.J., 2008. A theoretical and numerical study of urban heat island–induced circulation and convection. *Journal of the Atmospheric Sciences*, *65*(6), pp.1859–1877.

Hassim, M.E.E., Lane, T.P. and Grabowski, W.W., 2016. The diurnal cycle of rainfall over New Guinea in convection-permitting WRF simulations. *Atmos. Chem. Phys*, *16*(1), pp.161–175.

He, H. and Zhang, F., 2010. Diurnal variations of warm-season precipitation over northern China. *Monthly Weather Review*, *138*(4), pp.1017–1025.

Hong, S.Y., Dudhia, J. and Chen, S.H., 2004. A revised approach to ice microphysical processes for the bulk parameterization of clouds and precipitation. *Monthly Weather Review*, *132*(1), pp.103–120.

Hong, S.Y., Noh, Y. and Dudhia, J., 2006. A new vertical diffusion package with an explicit treatment of entrainment processes. *Monthly Weather Review*, *134*(9), pp.2318–2341.

Huffman, G.J., Bolvin, D.T., Nelkin, E.J., Wolff, D.B., Adler, R.F., Gu, G., Hong, Y., Bowman, K.P. and Stocker, E.F., 2007. The TRMM multisatellite precipitation analysis (TMPA): Quasi-global, multiyear, combined-sensor precipitation estimates at fine scales. *Journal of Hydrometeorology*, *8*(1), pp.38–55.

~~Jeong, J.H., Walther, A., Nikulin, G., Chen, D. and Jones, C., 2011. Diurnal cycle of precipitation amount and frequency in Sweden: observation versus model simulation. *Tellus A*, *63*(4), pp.664-674.~~

Iacono, M.J., Delamere, J.S., Mlawer, E.J., Shephard, M.W., Clough, S.A. and Collins, W.D., 2008. Radiative forcing by long-lived greenhouse gases: Calculations with the AER radiative transfer models. *Journal of Geophysical Research: Atmospheres*, *113*(D13).

Joyce, R.J., Janowiak, J.E., Arkin, P.A. and Xie, P., 2004. CMORPH: A method that produces global precipitation estimates from passive microwave and infrared data at high spatial and temporal resolution. *Journal of Hydrometeorology*, *5*(3), pp.487–503.

Keenan, T.D., Holland, G.J., Manton, M.J. and Simpson, J., 1988. TRMM ground truth in a monsoon environment: Darwin, Australia. *Australian Meteorological Magazine*, *36*(2), p.81.

Kishtawal, C.M. and Krishnamurti, T.N., 2001. Diurnal variation of summer rainfall over Taiwan and its detection using TRMM observations. *Journal of Applied Meteorology*, *40*(3), pp.331-344.

Liang, Z. and Wang, D., 2016. Sea breeze and precipitation over Hainan Island. *Quarterly Journal of the Royal Meteorological Society*.

Mapes, B.E., Warner, T.T. and Xu, M., 2003. Diurnal patterns of rainfall in northwestern South America. Part III: Diurnal gravity waves and nocturnal convection offshore. *Monthly Weather Review*, *131*(5), pp.830–844.

Neale, R. and Slingo, J., 2003. The maritime continent and its role in the global climate: A GCM study. *Journal of Climate*, *16*(5), pp.834–848.

Nguyen, H., Protat, A., Kumar, V., Rauniyar, S., Whimpey, M. and Rikus, L., 2015. A regional forecast model evaluation of statistical rainfall properties using the CPOL radar observations in different precipitation regimes over Darwin, Australia. *Quarterly Journal of the Royal Meteorological Society*, *141*(691), pp.2337–2349.

Ogino, S.Y., Yamanaka, M.D., Mori, S. and Matsumoto, J., 2016. How Much is the Precipitation Amount over the Tropical Coastal Region?. *Journal of Climate*, *29*(3), pp.1231–1236.

Qian, J.H., 2008. Why precipitation is mostly concentrated over islands in the Maritime Continent. *Journal of the Atmospheric Sciences*, *65*(4), pp.1428–1441.

Skamarock, W.C., Klemp, J.B., Dudhia, J., Gill, D.O., Barker, D.M., Duda, M.G., Huang, X.Y., Wang, W. and Jordan, G., *Powers. 2008. A Description of the Advanced Research WRF Version 3. NCAR Technical Note*. NCAR/TN–475+ STR.

Sobel, A.H., Burleyson, C.D. and Yuter, S.E., 2011. Rain on small tropical islands. *Journal of Geophysical Research: Atmospheres*, *116*(D8).

Sun, J. and Zhang, F., 2012. Impacts of mountain–plains solenoid on diurnal variations of rainfalls along the mei-yu front over the east China plains. *Monthly Weather Review*, *140*(2), pp.379–397.

Trier, S.B., Davis, C.A. and Ahijevych, D.A., 2010. Environmental controls on the simulated diurnal cycle of warm-season precipitation in the continental United States. *Journal of the Atmospheric Sciences*, *67*(4), pp.1066–1090.

Tu, X., Zhou, M.Y., Z. and Sheng, S.H., 1993. The mesoscale numerical simulation of the flow field of the Hainan Island and the Leizhou Peninsula. *Acta Oceanolog (in Chinese)*, *12*(2), pp.219–235.

Wapler, K. and Lane, T.P., 2012. A case of offshore convective initiation by interacting land breezes near Darwin, Australia. *Meteorology and Atmospheric Physics*, *115*(3–4), pp.123–137.

Yang, G.Y. and Slingo, J., 2001. The diurnal cycle in the tropics. *Monthly Weather Review*, *129*(4), pp.784–801.

~~Yin, S., Chen, D. and Xie, Y., 2009. Diurnal variations of precipitation during the warm season over China. *International Journal of Climatology*, *29*(8), pp.1154–1170.~~

~~Zhang, G., Cook, K.H. and Vizy, E.K., 2016. The diurnal cycle of warm season rainfall over West Africa. Part I: Observational analysis. *Journal of Climate*, *29*(23), pp.8423–8437.~~

~~Zhang, G., Cook, K.H. and Vizy, E.K., 2016. The diurnal cycle of warm season rainfall over West Africa. Part II: Convection-permitting simulations. *Journal of Climate*, *29*(23), pp.8439–8454.~~

Zhai, W., Li, G., Sun, B. and Dang, R., 1998. Varying season's mesoscale wind field circulation in Hainan island. J. Trop. Meteorol. 4: 79–87.

Zhang, Y., Zhang, F. and Sun, J., 2014. Comparison of the diurnal variations of warm-season precipitation for East Asia vs. North America downstream of the Tibetan Plateau vs. the Rocky Mountains. *Atmospheric Chemistry and Physics*, *14*(19), pp.10741–10759.

Figure Captions

FIG. 1. Configuration of model domain, gauge-based station points (color dots correspond to the time series shown in Fig. 2) over Hainan Island and the terrain height (shading, m). The red ellipse is the idealized representation of the island (used for the idealized simulations), and the red vertical line indicates the location of the vertical cross-sections shown in Figs. 14– and 16.

FIG. 2. Average rainfall accumulations by hour, each month of the year, obtained from the rain gauge network. The color is consistent with the color dots over the island in Fig. 1. LST means the Local Standard Time.

FIG. 3. Average station rainfall accumulations obtained from gauges (blue) and CMORPH (red) in each month.

FIG. 4. Fraction of the total precipitation that can be attributed to the diurnal cycle, by month (shading), along with average hourly precipitation accumulations (black contours every 0.05 mm, starting at 0.25 mm).

FIG. 5. Average rainfall accumulations by hour in May and June (a) from rain gauges and (b) derived from CMORPH.

FIG. 6. Ten-year average, hourly rainfall accumulations at 3-h intervals for May and June derived from CMORPH (shading) except used 1700 LST as it is the strongest rainfall time in CMORPH observation. Three-year average wind velocity (vectors) is also shown. Rain gauge locations are indicated in (a).

FIG. 7. The average of 2-meter temperature (T2_avg), 2-meter temperature tendency (T2_tendency, temperature difference between two neighboring hours), and hourly rainfall accumulation over the island based on (a) gauge observations, (b) simulation REAL, (c) simulation NoTER, (d) and simulation IDEAL. Horizontal colored lines indicate means over all hours.

FIG. 8. Hourly precipitation accumulation (shading) and average perturbation wind (vectors) on the second lowest model level for horizontal wind in simulation REAL every 3 h. The averages over all hours are shown in (a).

FIG. 9. As in FIG. 8, but for simulation NoTER.

FIG. 10. As in FIG. 8, but for simulation IDEAL.

FIG. 11. Water vapor mixing ratio (shading) and horizontal wind (vectors) at 850 hPa, and hourly precipitation accumulations > 0.1 mm (thick purple contours), (b–i) every 3 h and (a) averaged over all times.

FIG. 12. (a) 2-meter mean temperature (shading) and horizontal wind (vectors) on the second lowest model level for horizontal wind; (b–i) 2-meter mean temperature perturbation (shading)

and mean perturbation horizontal wind (vectors) on the second lowest model level every 3 h. The right color bar is used for (a).

FIG. 13. Cloud water mixing ratio (red shading), 2-meter temperature (grey shaded), perturbation horizontal wind on the second lowest model level for horizontal wind (yellow vectors), and hourly precipitation accumulation (green contour lines) every 3 h.

FIG. 14. Vertical cross-sections of ~~water vapor mixing ratio~~relative humidity (shading), perturbation wind (vectors; the scale of the vertical component is increased by a factor of 5), and temperature (contours) in the south-to-north direction (see red line in Fig. 1) averaged over all hours (a) and at 3-h intervals (b–i). The triangles in each panel indicate the edges of the island.

FIG. 15. ~~Vertical cross-sections of perturbation temperature (shading), perturbation wind (vectors; the scale of the vertical component is increased by a factor of 5), and temperature (contours) in the south-to-north direction (see red line in Fig. 1) averaged over all hours (a) and at 3-h intervals (b–i). The triangles in each panel indicate the edges of the island~~Horizontal temperature advection (shaded) and horizontal wind (vector, m s^{-1}) on the first model level in simulation IDEAL.

FIG. ~~Fig. 16. As in Fig. 12, but for simulation Fakedry.~~

~~Fig. 17. As in Fig. 8, but for simulation Fakedry.~~

~~Fig. 18.~~16. Hovmoller diagrams of perturbation meridional wind component on the second lowest model level for horizontal wind (shading) in the (a) IDEAL ~~and~~, (b) Fakedry and (c) NOVAP simulations, respectively. Precipitation exceeding 0.1 mm h^{-1} is enclosed by the heavy purple contours. The two vertical dash lines indicate the edges of the island.

~~Fig. 19. As in Fig. 15, but for simulation Fakedry.~~

797
798
799
800
801
802
803
804
805
806

807

Table 1

Station observation period used over Hainan Island

Station No.	Latitude	Longitude	Height (m)	Obs period(YearMonth)	Name
59757	20	110.37	9.9	197701-201212	Qiongshan
59758	20	110.25	63.5	195101-201212	Haikou
59838	19.1	108.62	7.6	195506-201212	Dongfang
59842	19.9	109.68	31	196201-201212	Lingao
59843	19.73	110	31.4	195901-201212	Dengmai
59845	19.52	109.58	169	195505-201212	Zanzhou
59847	19.27	109.05	98.1	196605-201212	Changjiang
59848	19.23	109.43	215.6	196201-201212	Baisha
59849	19.03	109.83	250.9	195602-201212	Qiongzhong
59851	19.7	110.33	24.2	196301-201212	Dingan
59854	19.37	110.1	118.3	196301-201212	Tunchang
59855	19.23	110.47	24	195509-201212	Qiaonghai
59856	19.62	110.75	21.7	195901-201212	Wenchang
59940	18.75	109.17	155	196202-201212	Ledong
59941	18.77	109.52	328.5	196301-201212	Wuzhishan
59945	18.65	109.7	68.6	196509-201212	Baoting
59948	18.22	109.58	419.4	196201-201212	Sanya
59951	18.8	110.33	39.9	196201-201212	Wanning
59954	18.5	110.03	13.9	195601-201212	Lingshui

822

823 **Figures**

824
825
826

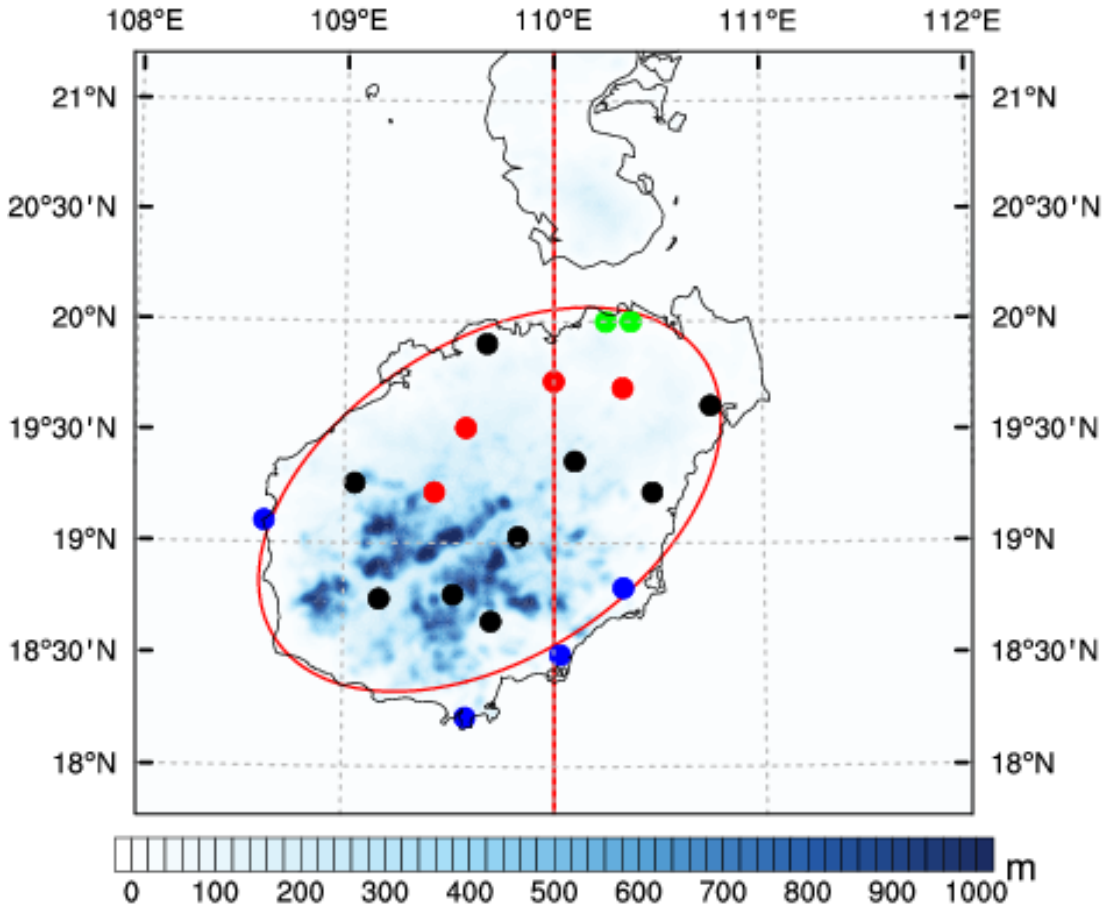

827

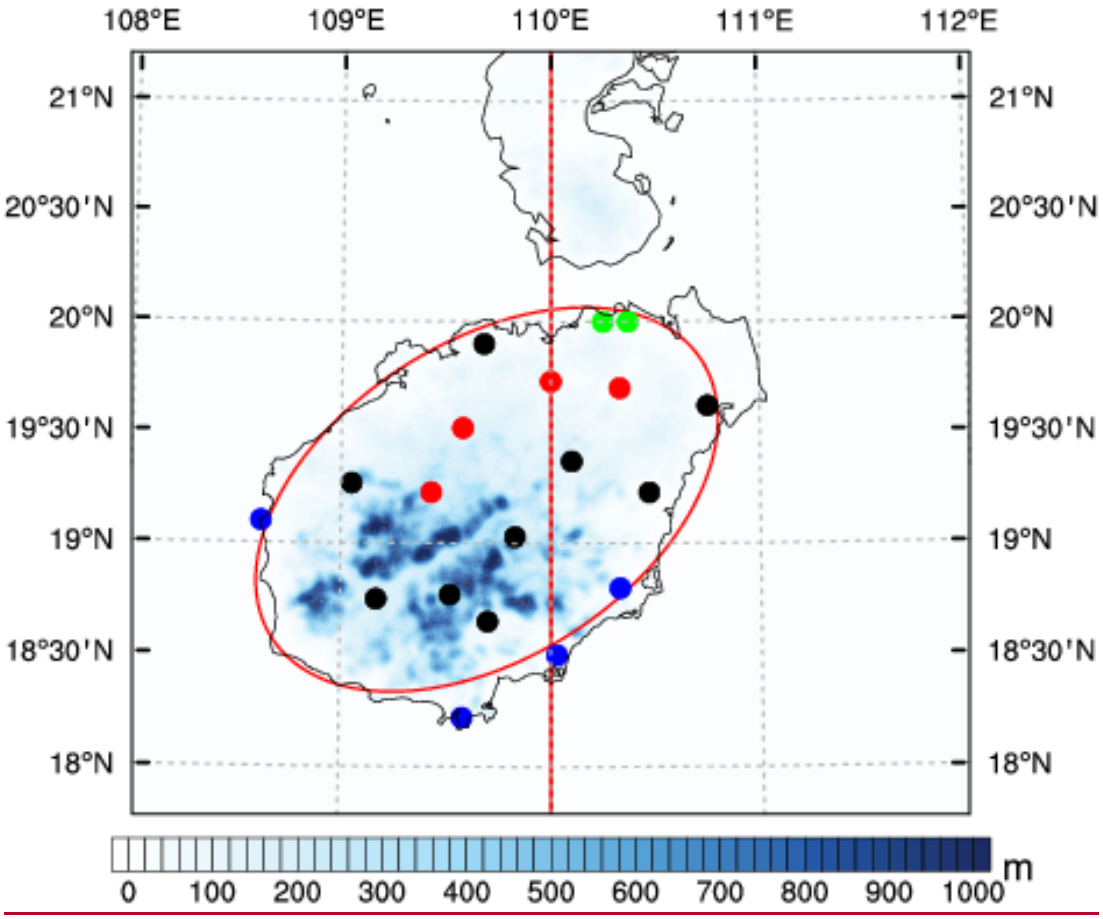

FIG. 1. Configuration of model domain, gauge-based station points (color dots correspond to the time series shown in Fig. 2) over Hainan Island and the terrain height (shading, m). The red ellipse is the idealized representation of the island (used for the idealized simulations), and the red vertical line indicates the location of the vertical cross-sections shown in Figs. 14– and 16.

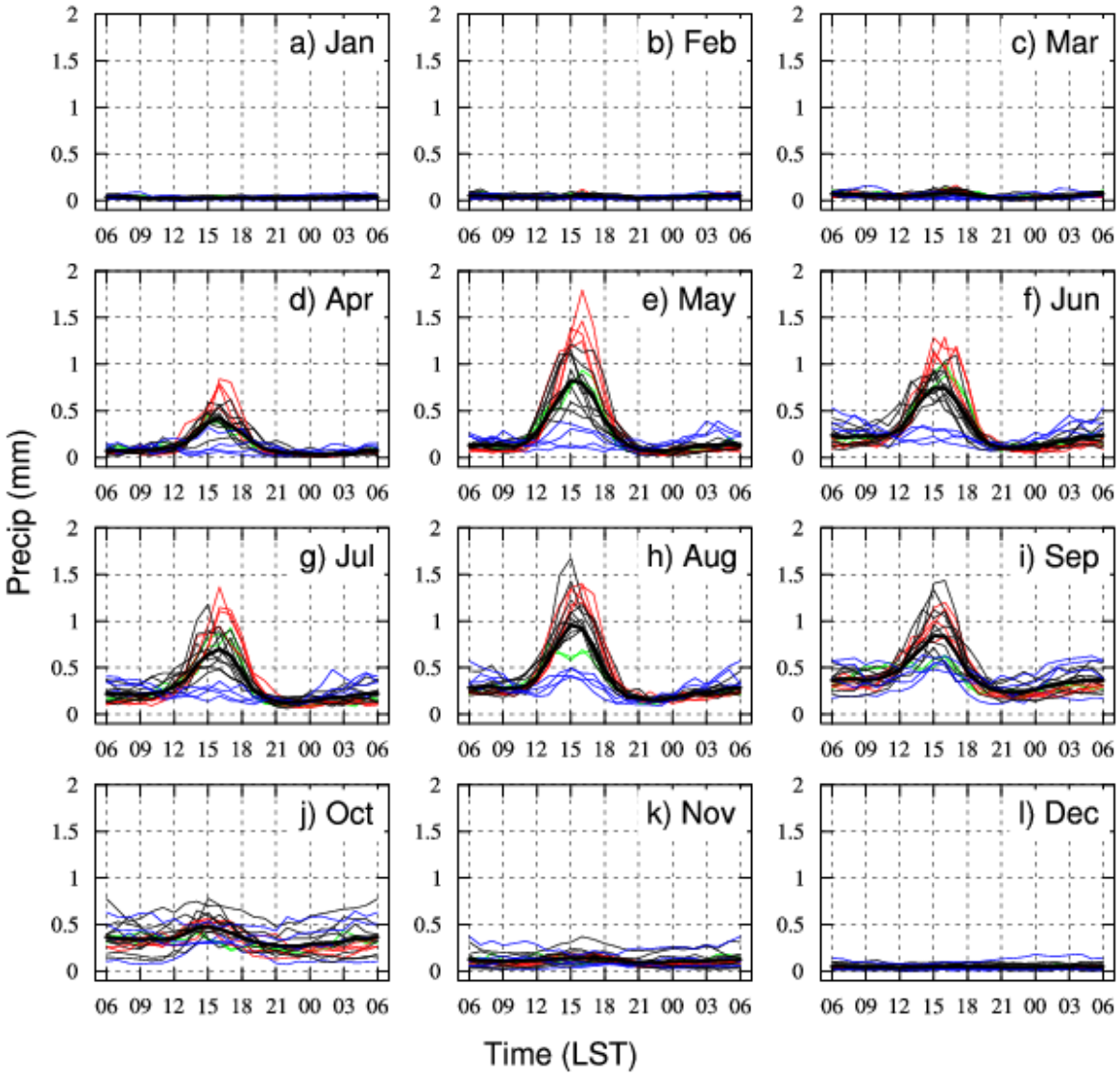
a) Jan
b) Feb
c) Mar
d) Apr
e) May
f) Jun
g) Jul
h) Aug
i) Sep
j) Oct
k) Nov
l) Dec
Precip (mm)
Time (LST)
0
0.5
1
1.5
2
06 09 12 15 18 21 00 03 06

842

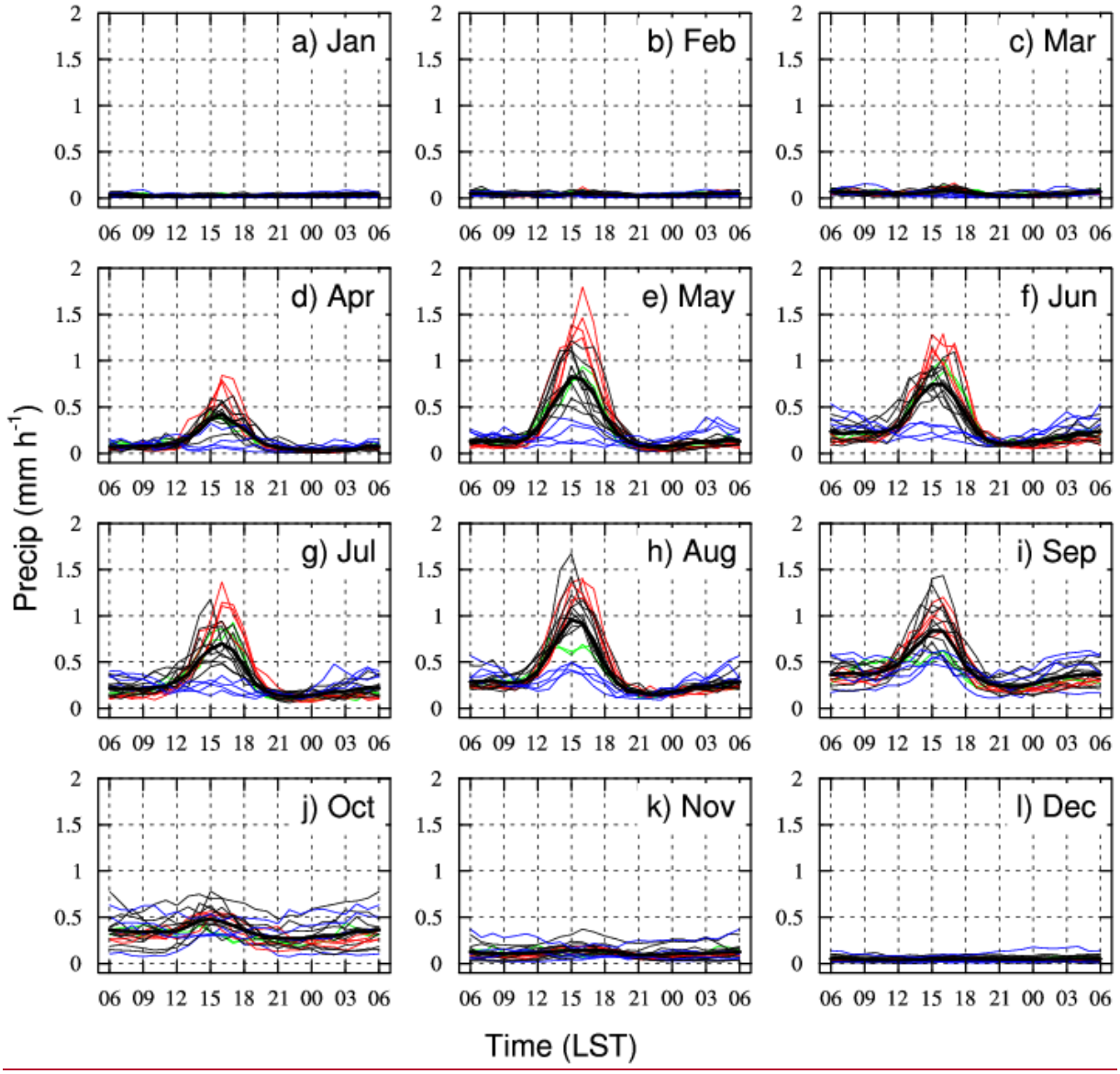

FIG. 2. Average rainfall accumulations by hour, each month of the year, obtained from the rain gauge network. The color is consistent with the color dots over the island in Fig. 1. LST means the Local Standard Time.

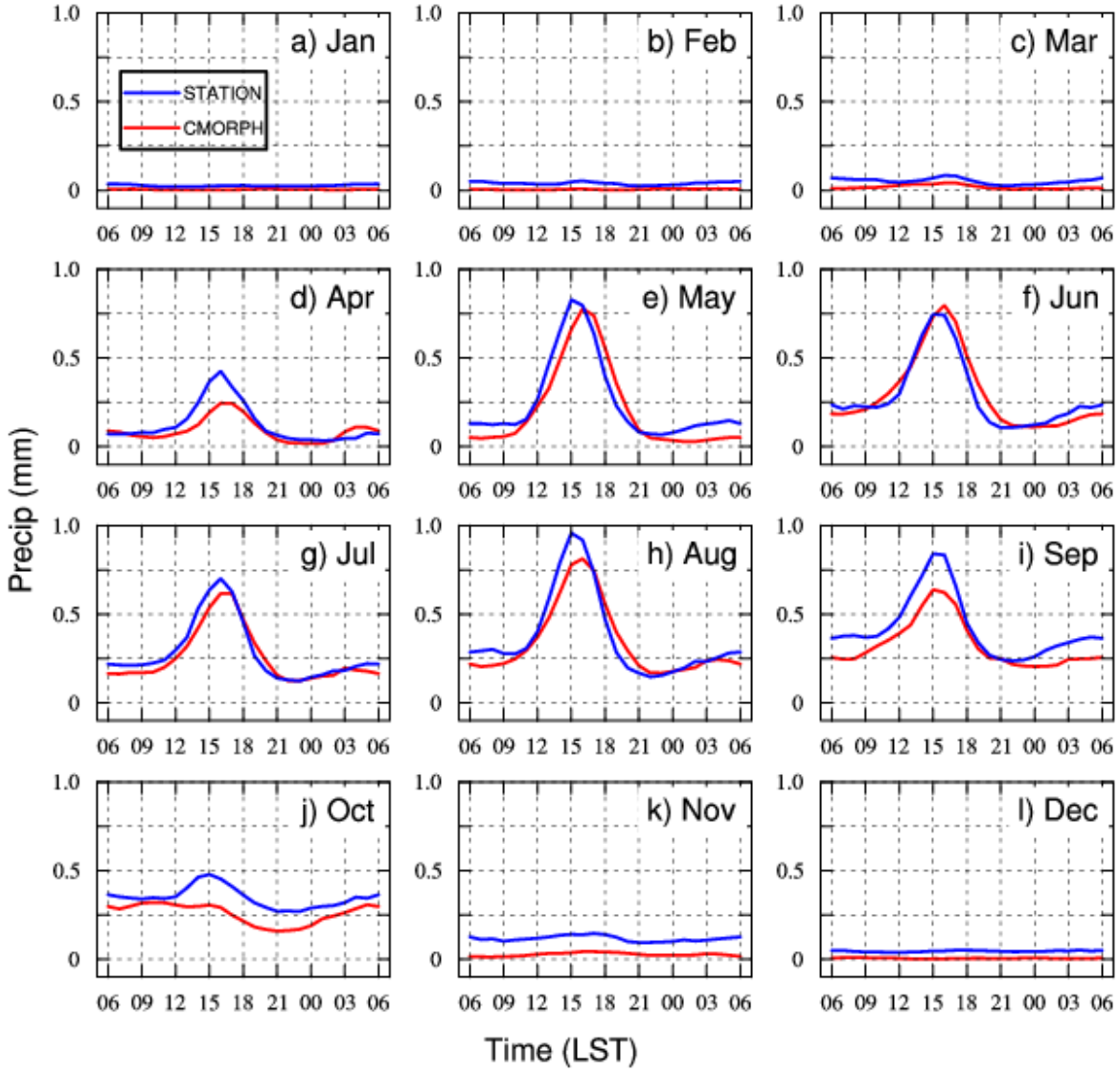
a) Jan
b) Feb
c) Mar
d) Apr
e) May
f) Jun
g) Jul
h) Aug
i) Sep
j) Oct
k) Nov
l) Dec
STATION
CMORPH
Precip (mm)
Time (LST)
1.0
0.5
0
06 09 12 15 18 21 00 03 06

857

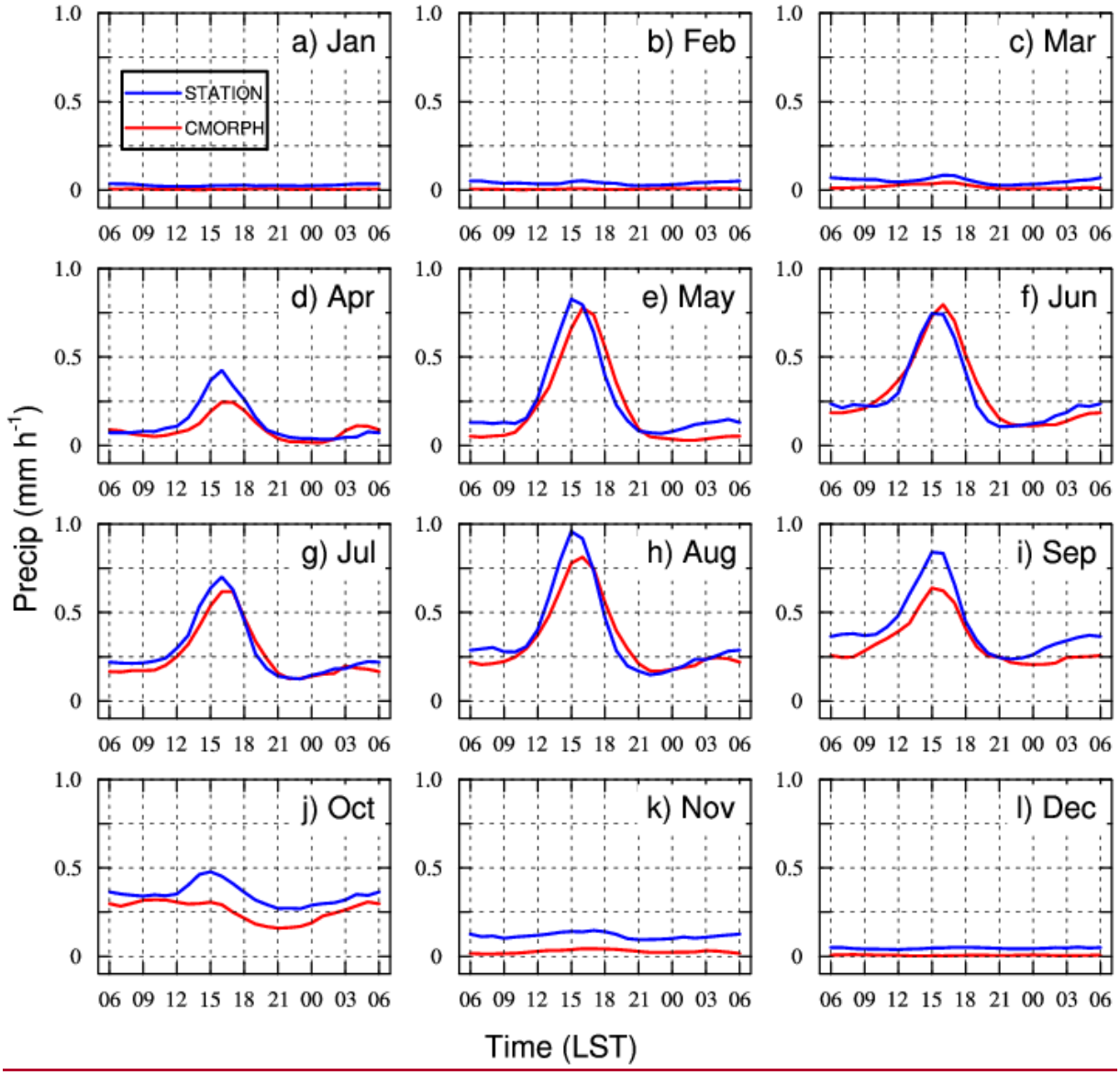

FIG. 3. ~~Average station~~Diurnal cycles of hourly average rainfall accumulations obtained from gauges (blue) and CMORPH (red) in each month.

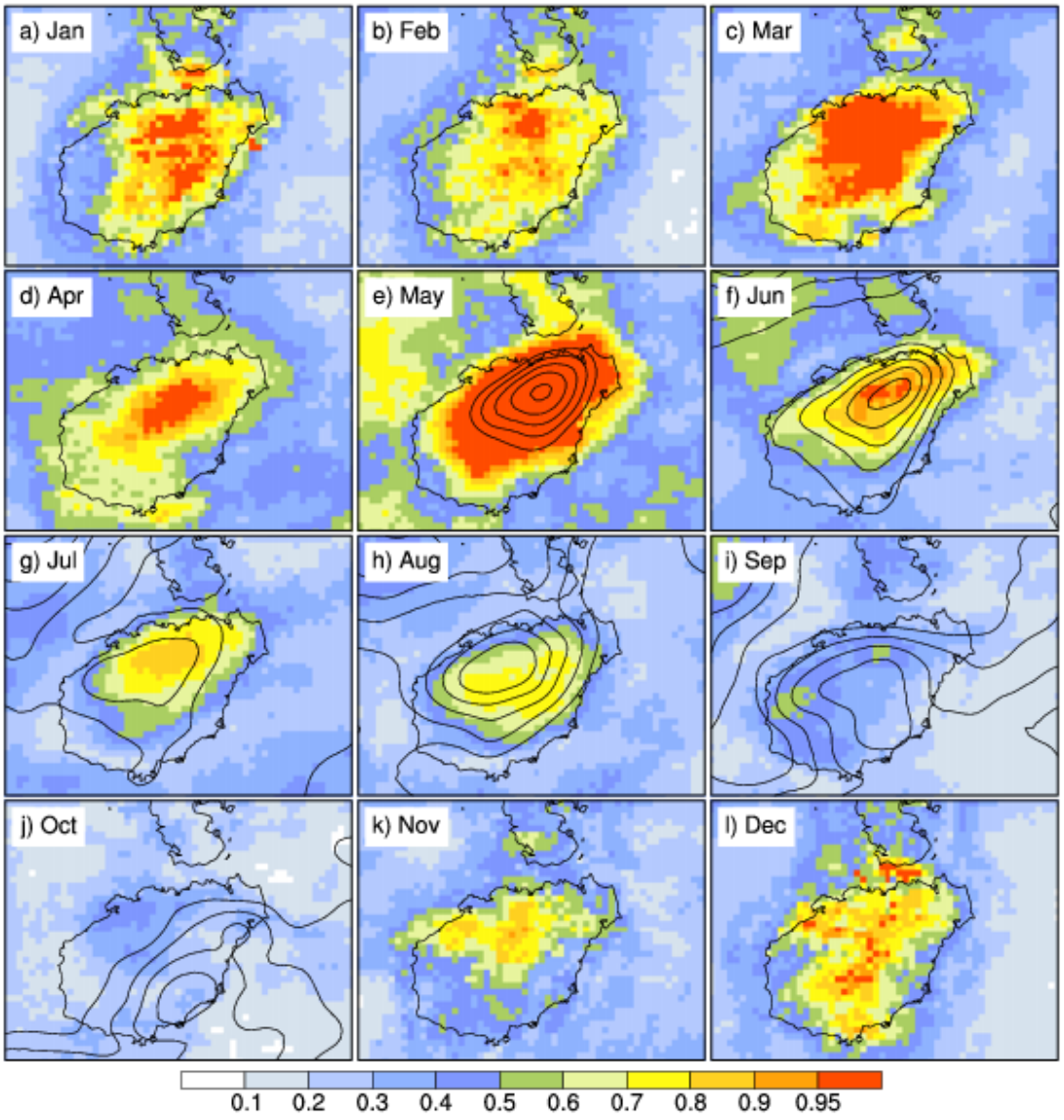
a) Jan
b) Feb
c) Mar
d) Apr
e) May
f) Jun
g) Jul
h) Aug
i) Sep
j) Oct
k) Nov
l) Dec
0.1
0.2
0.3
0.4
0.5
0.6
0.7
0.8
0.9
0.95

873

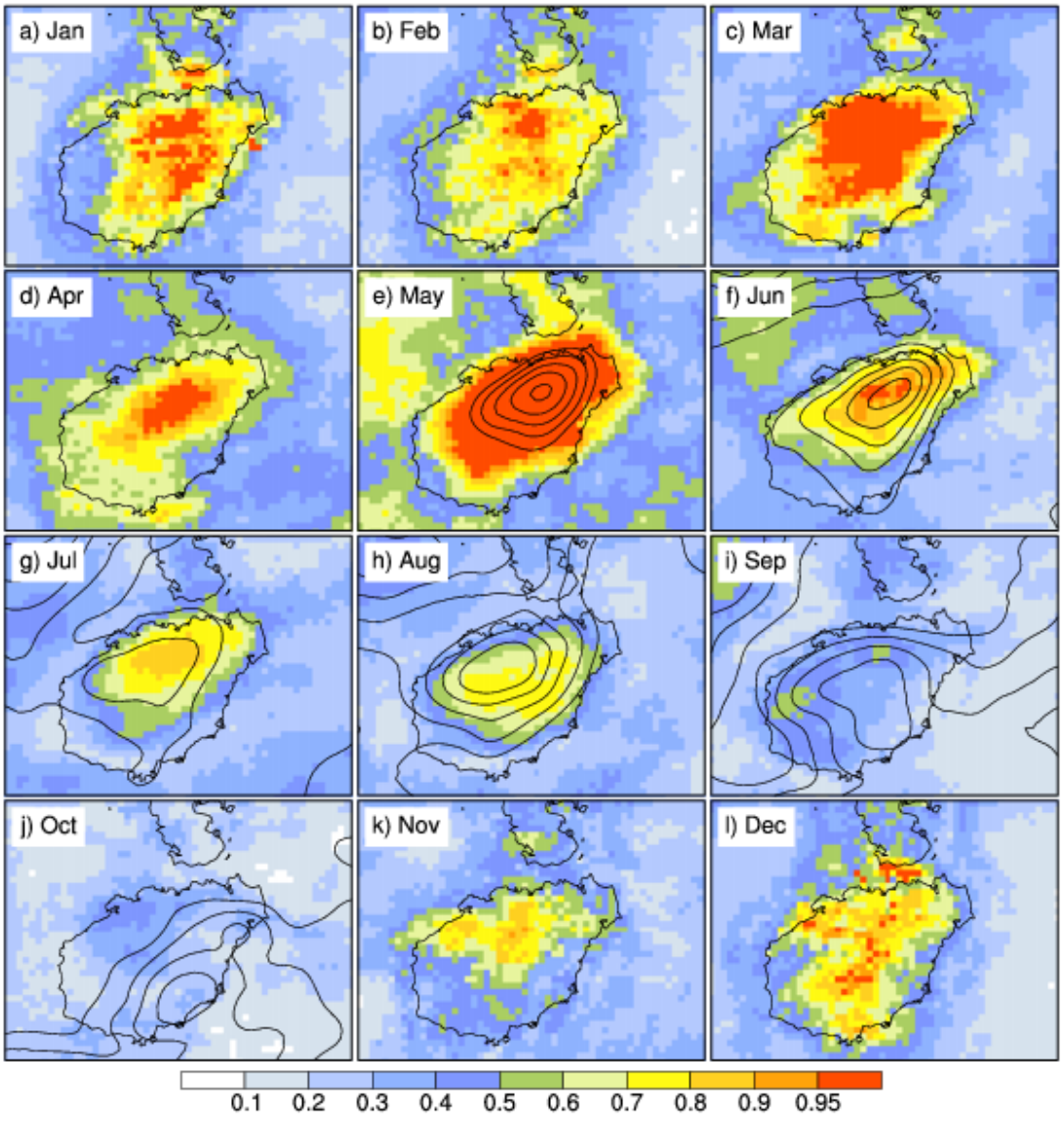

FIG. 4. Fraction of the total precipitation that can be attributed to the diurnal cycle, by month (shading), along with average hourly precipitation accumulations (black contours every 0.05 mm h^{-1}, starting at 0.25 mm h^{-1}).

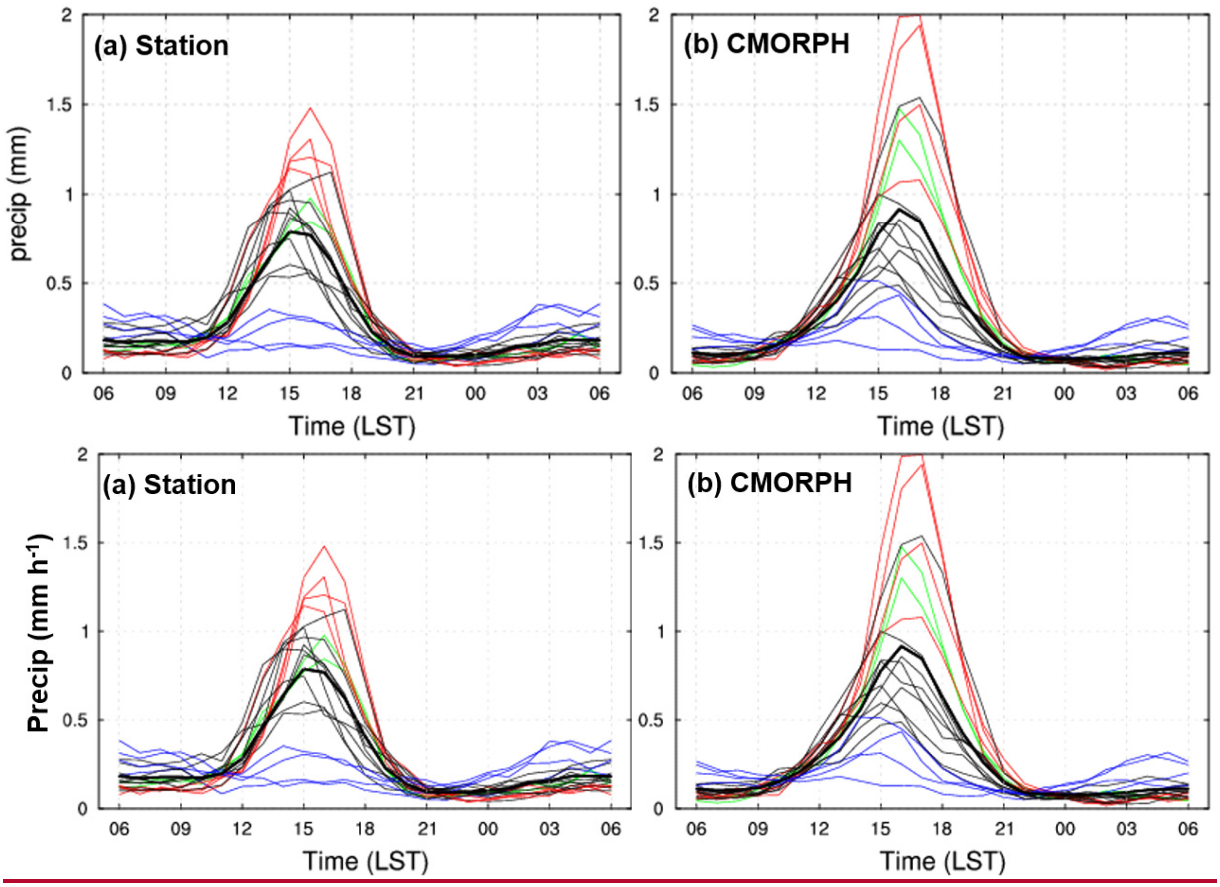

FIG. 5. Average rainfall accumulations by hour in May and June (a) from rain gauges and (b) derived from CMORPH.

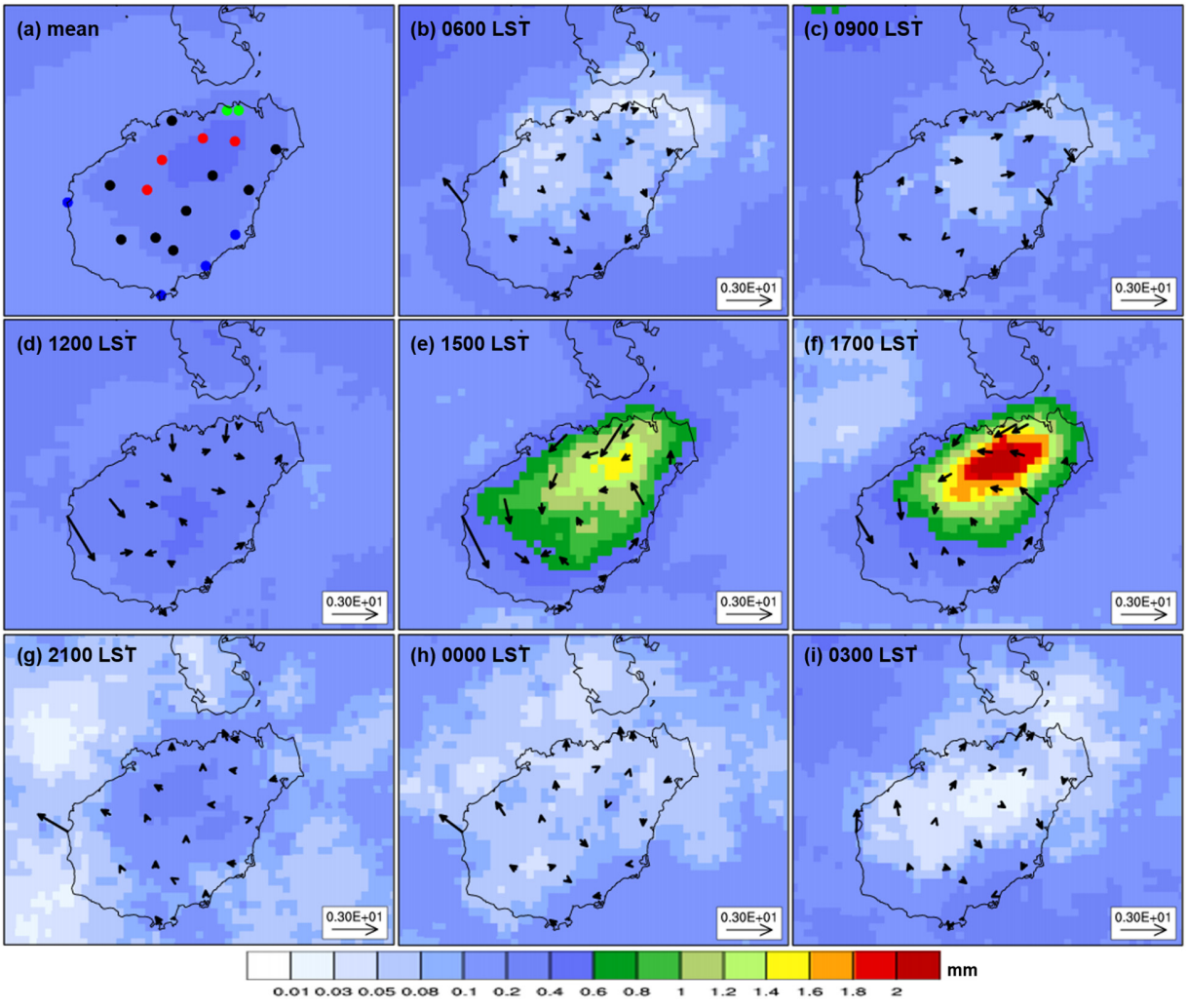
(a) mean
(b) 0600 LST
(c) 0900 LST
(d) 1200 LST
(e) 1500 LST
(f) 1700 LST
(g) 2100 LST
(h) 0000 LST
(i) 0300 LST
0.30E+01
mm
0.01 0.03 0.05 0.08 0.1 0.2 0.4 0.6 0.8 1 1.2 1.4 1.6 1.8 2

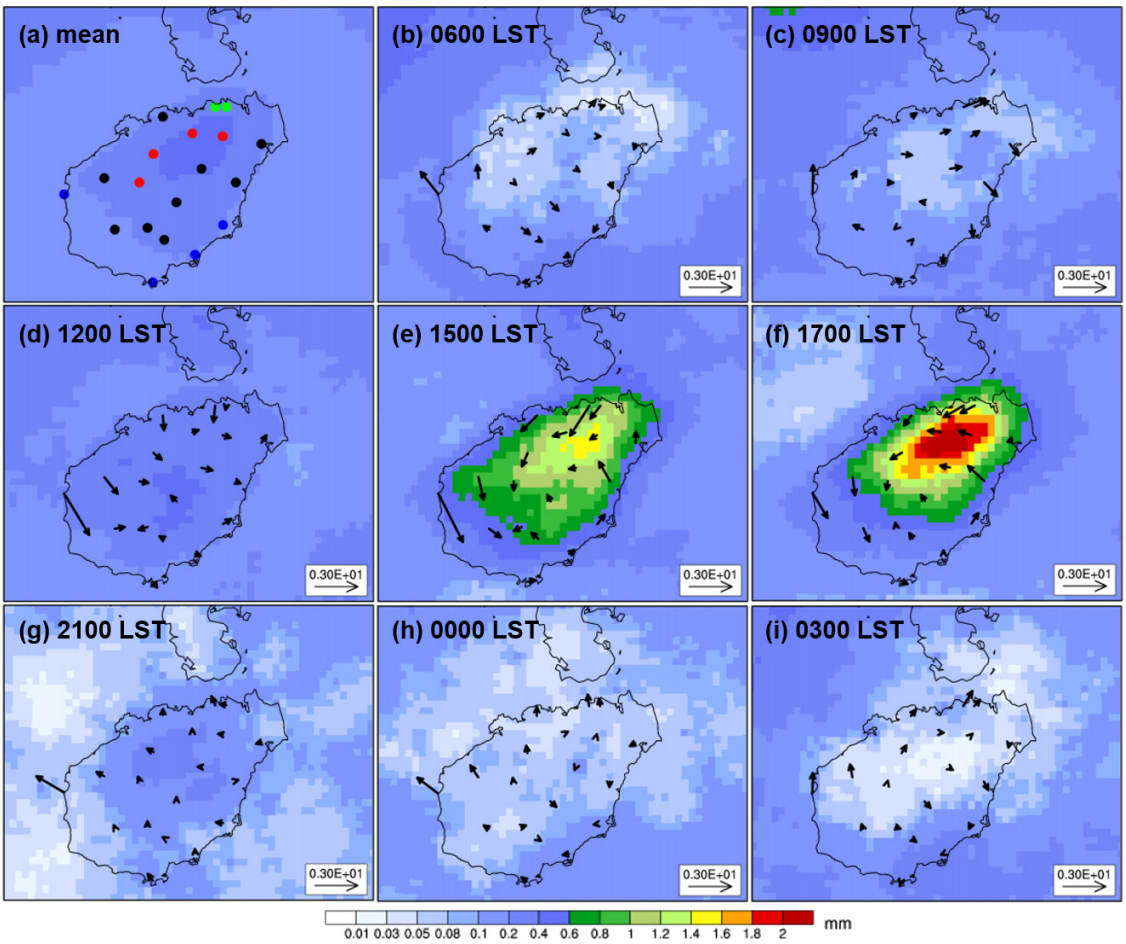

FIG. 6. Ten-year average, hourly rainfall accumulations at 3-h intervals for May and June derived from CMORPH (shading) except used 1700 LST as it is the strongest rainfall time in CMORPH observation. Three-year average wind velocity (vectors) is also shown. Rain gauge locations are indicated in (a).

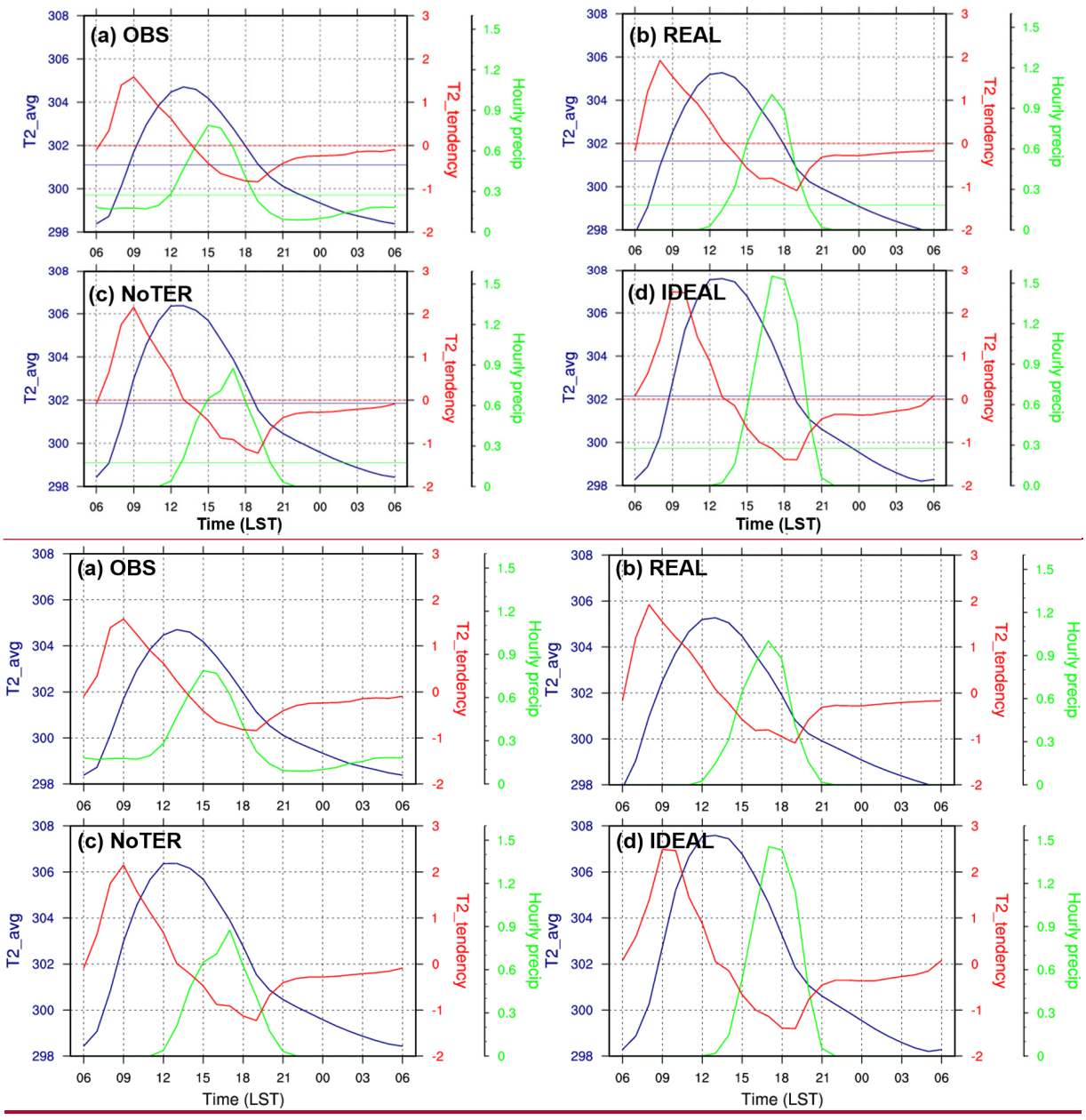

FIG. 7. The average of 2-meter temperature (T2_avg), 2-meter temperature tendency (T2_tendency, temperature difference between two neighboring hours), and hourly rainfall accumulation over the island based on (a) gauge observations, (b) simulation REAL, (c) simulation NoTER, (d) and simulation IDEAL. ~~Horizontal colored lines indicate means over all hours.~~

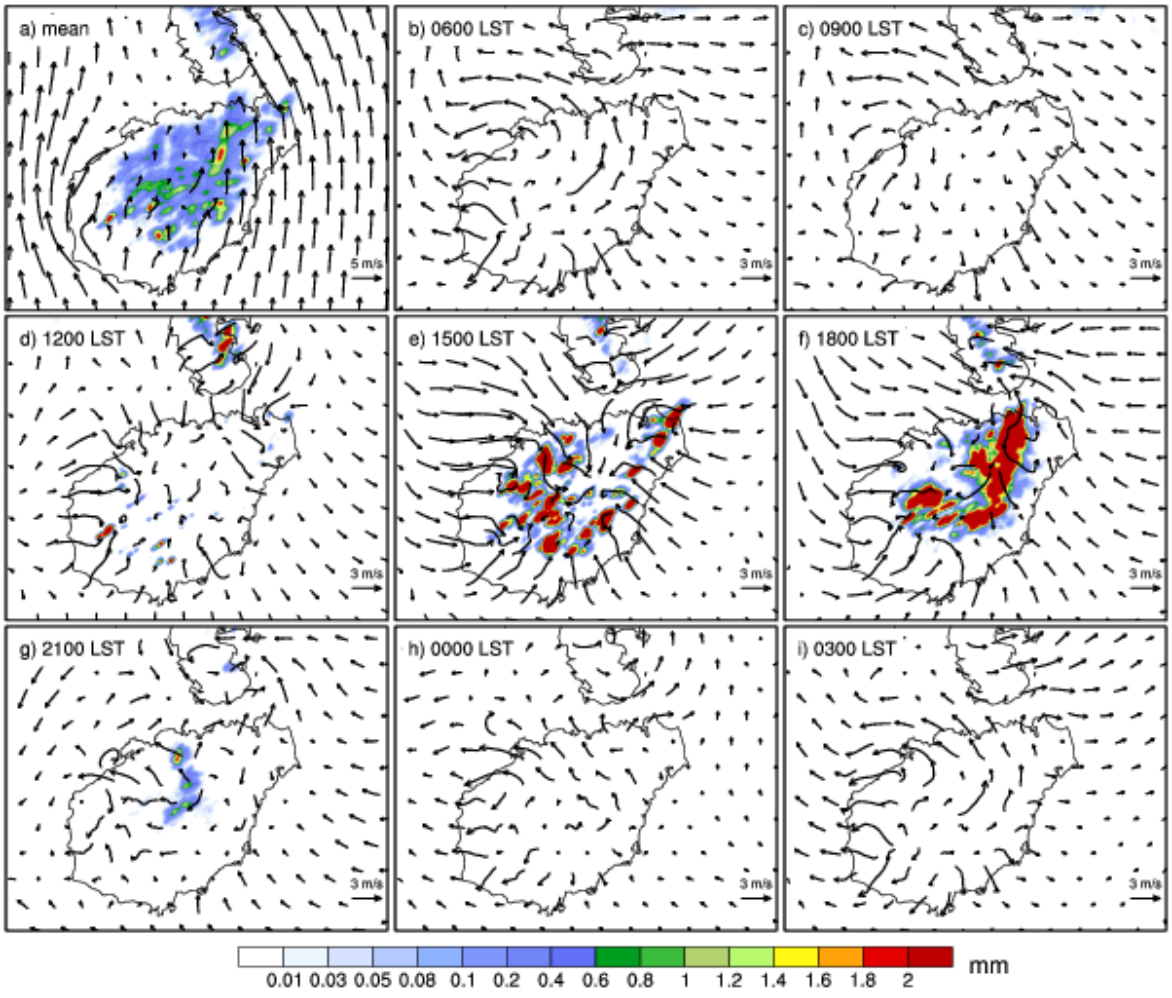
a) mean
b) 0600 LST
c) 0900 LST
d) 1200 LST
e) 1500 LST
f) 1800 LST
g) 2100 LST
h) 0000 LST
i) 0300 LST
5 m/s
3 m/s
0.01 0.03 0.05 0.08 0.1 0.2 0.4 0.6 0.8 1 1.2 1.4 1.6 1.8 2
mm

FIG. 8. Hourly precipitation accumulation (shading) and average perturbation wind (vectors) on the second lowest model level for horizontal wind in simulation REAL every 3 h. The averages over all hours are shown in (a).

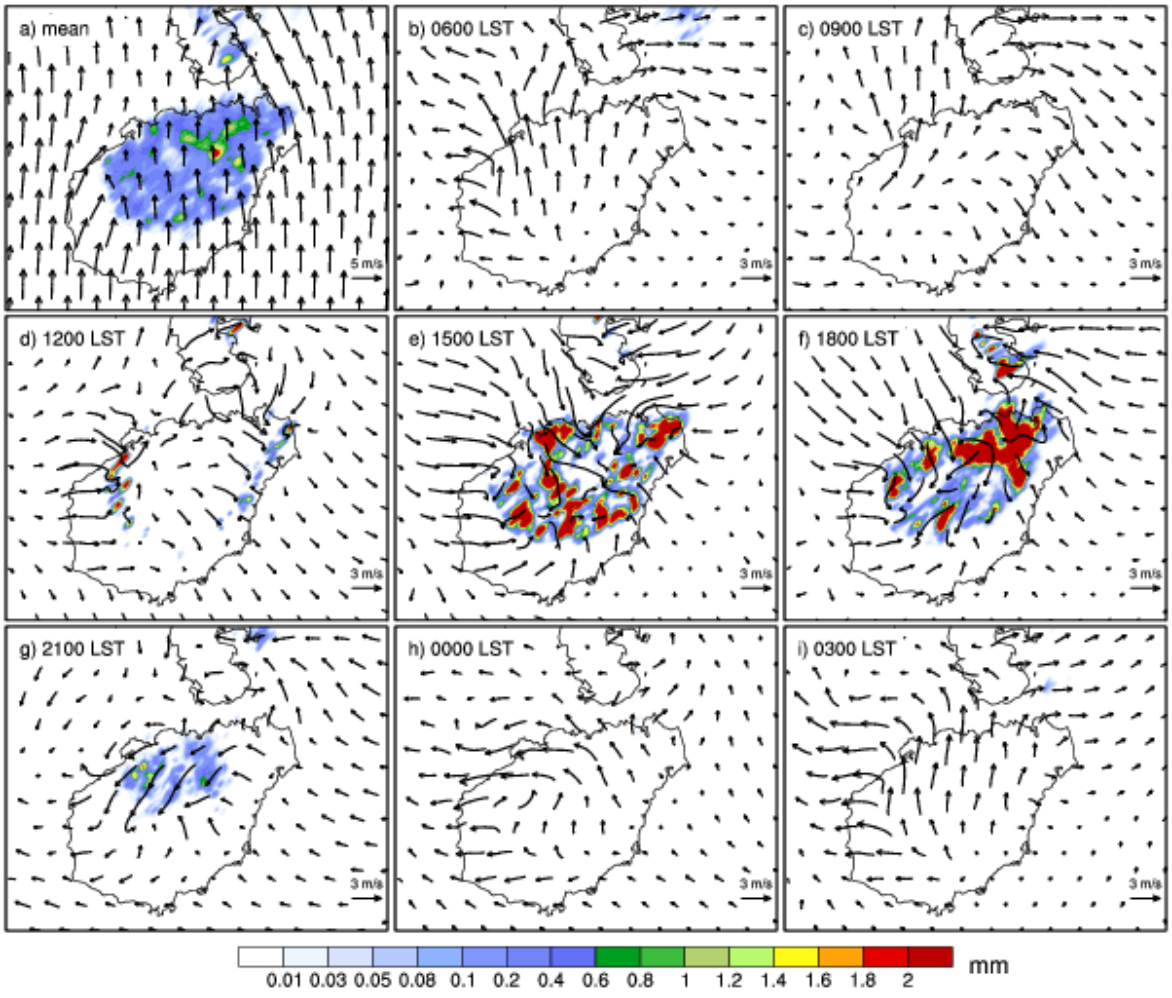

FIG. 9. As in FIG. 8, but for simulation NoTER.

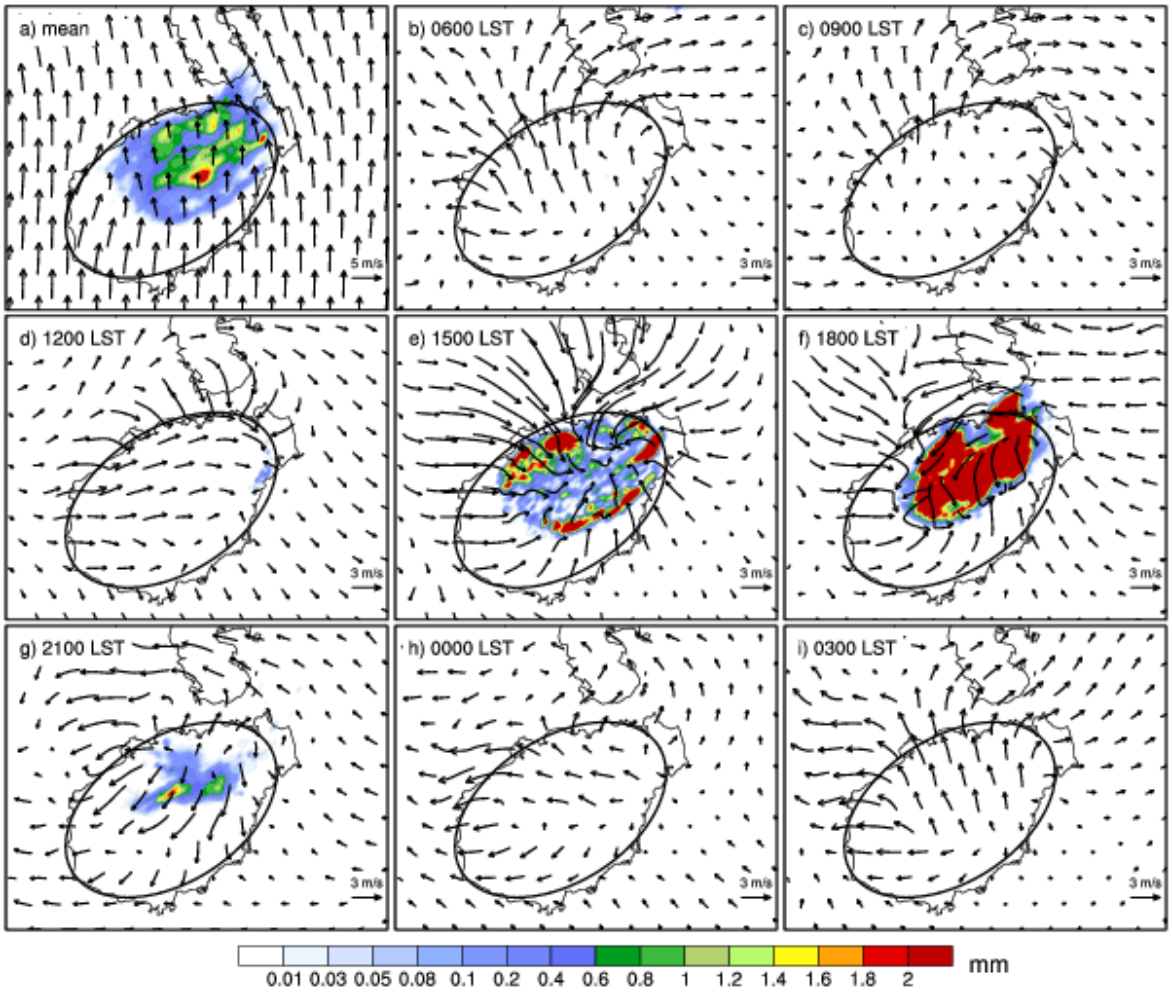

FIG. 10. As in FIG. 8, but for simulation IDEAL.

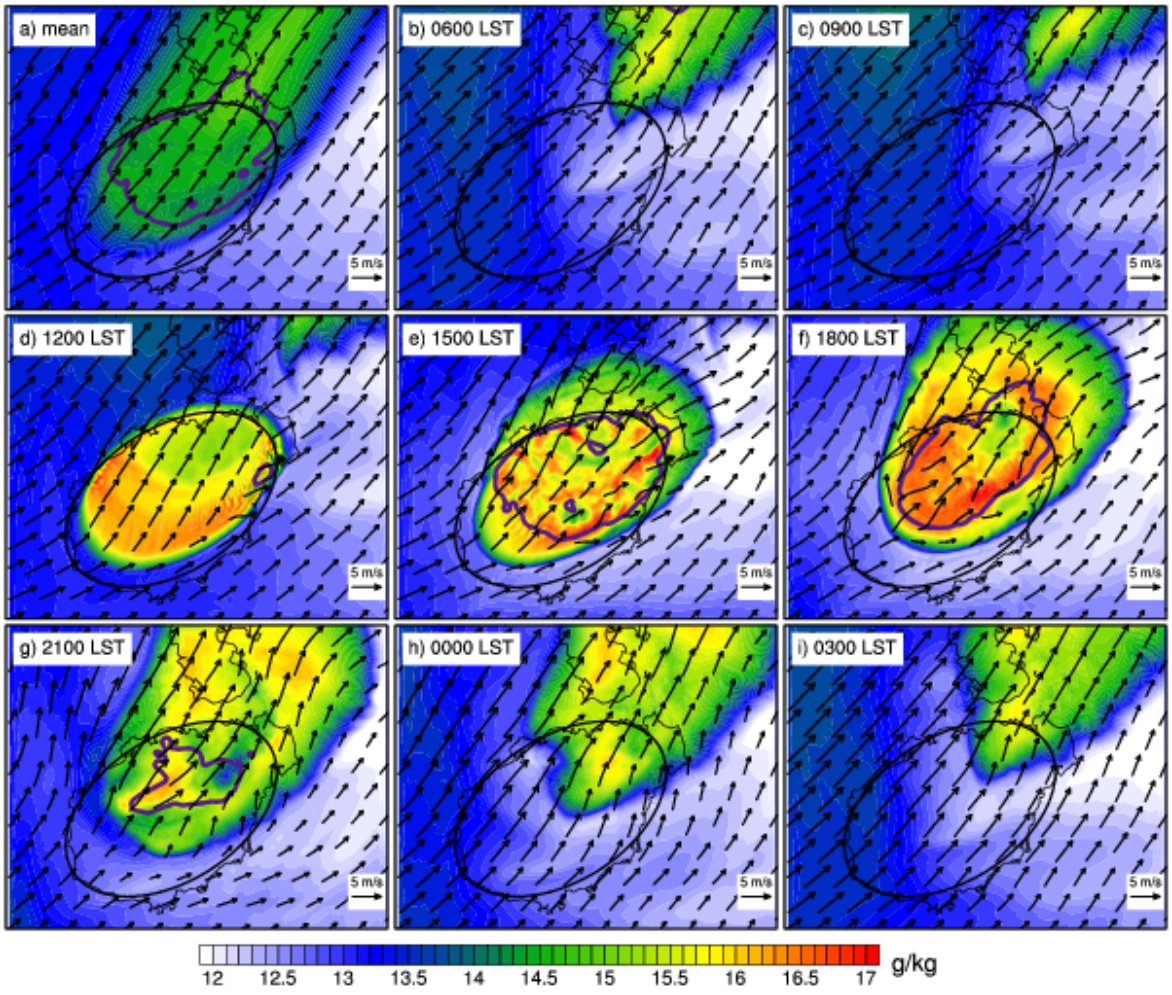
a) mean
b) 0600 LST
c) 0900 LST
d) 1200 LST
e) 1500 LST
f) 1800 LST
g) 2100 LST
h) 0000 LST
i) 0300 LST
5 m/s
12
12.5
13
13.5
14
14.5
15
15.5
16
16.5
17
g/kg

FIG. 11. Water vapor mixing ratio (shading) and horizontal wind (vectors) at 850 hPa, and hourly precipitation accumulations > 0.1 mm (thick purple contours), (b–i) every 3 h and (a) averaged over all times in IDEAL simulation.

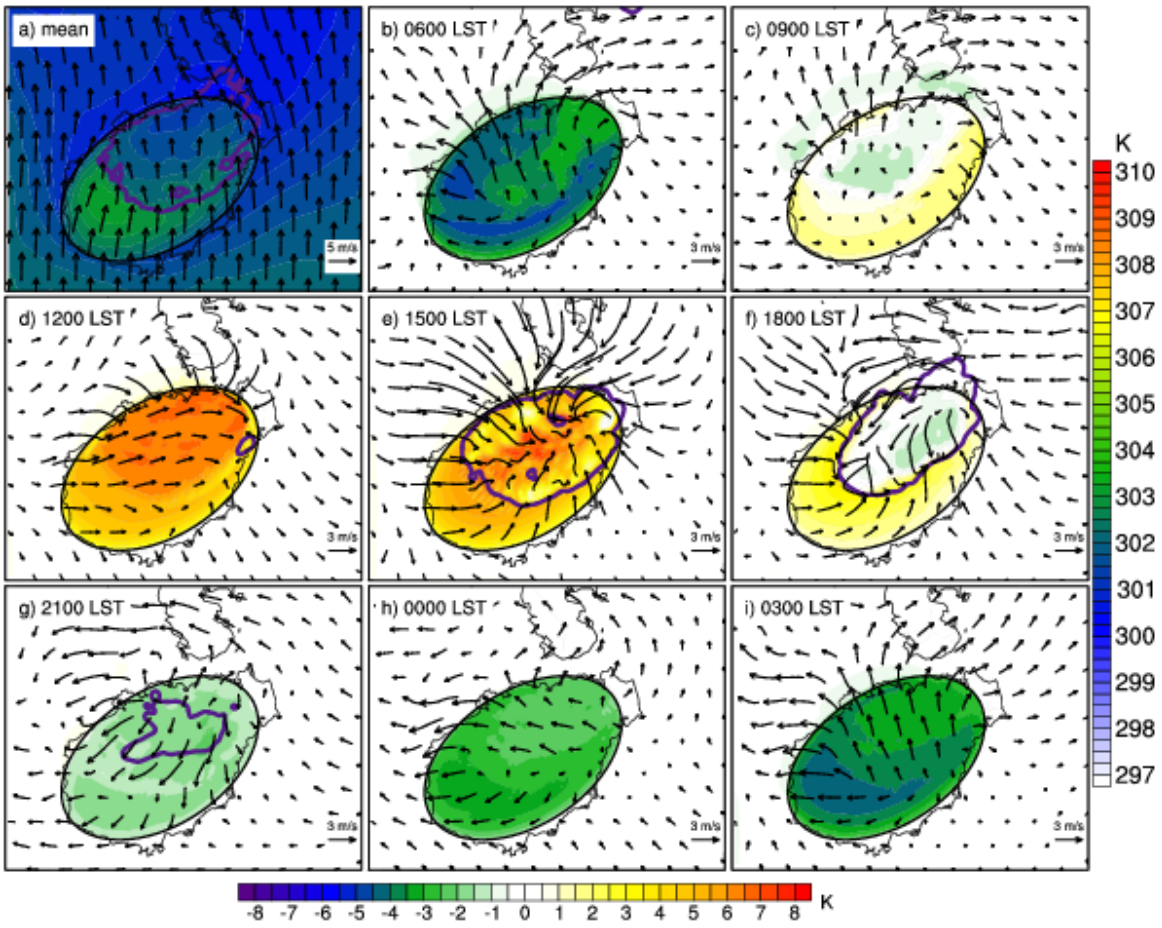

FIG. 12. (a) 2-meter mean temperature (shading) and horizontal wind (vectors) on the second lowest model level for horizontal wind; (b–i) 2-meter mean temperature perturbation (shading) and mean perturbation horizontal wind (vectors) on the second lowest model level every 3 h. in IDEAL simulation. The right color bar is used for (a).

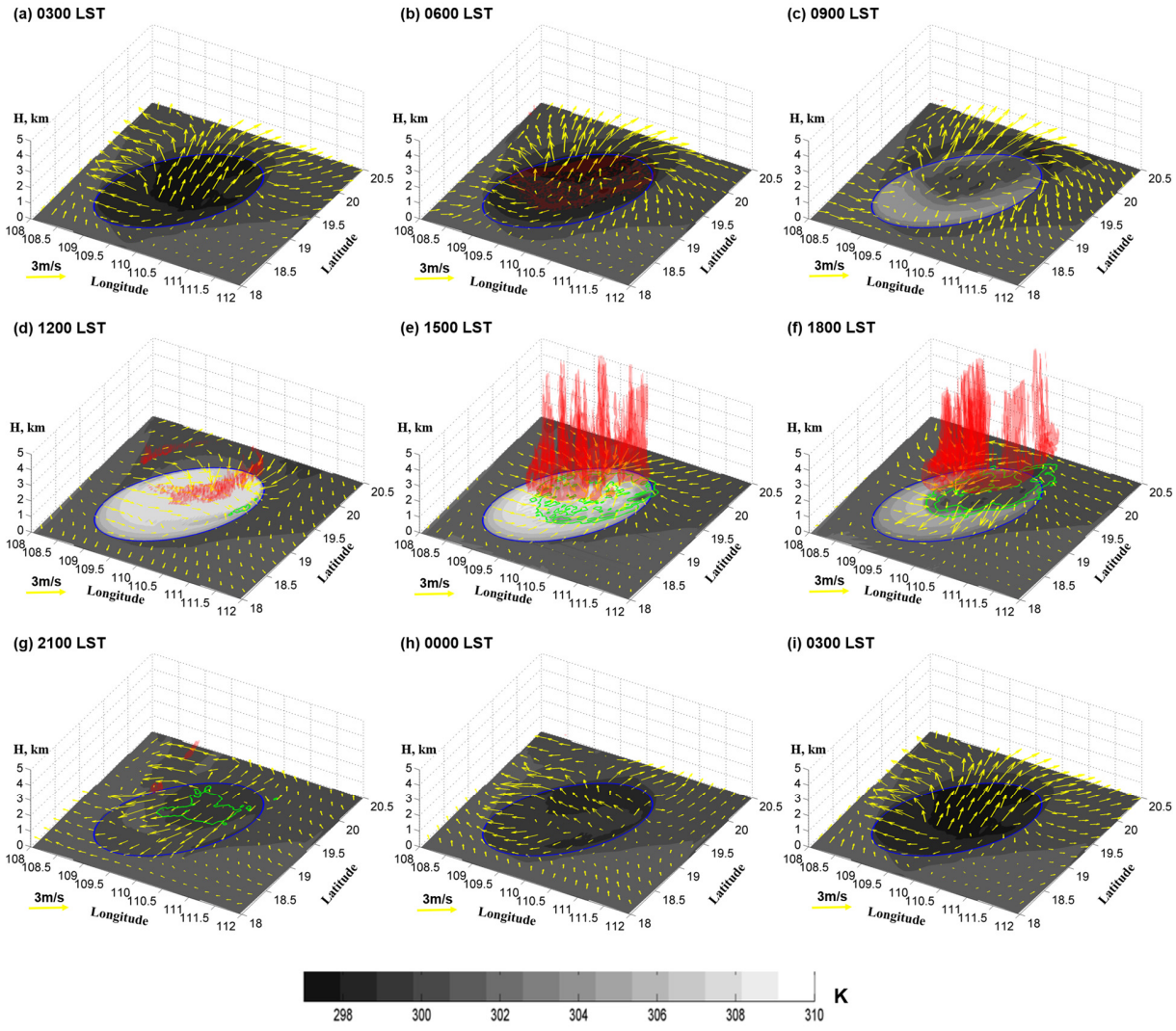

FIG. 13. Cloud water mixing ratio (red shading), 2-meter temperature (grey shaded), perturbation horizontal wind on the second lowest model level for horizontal wind (yellow vectors), and hourly precipitation accumulation (green contour lines) every 3 h in IDEAL simulation.

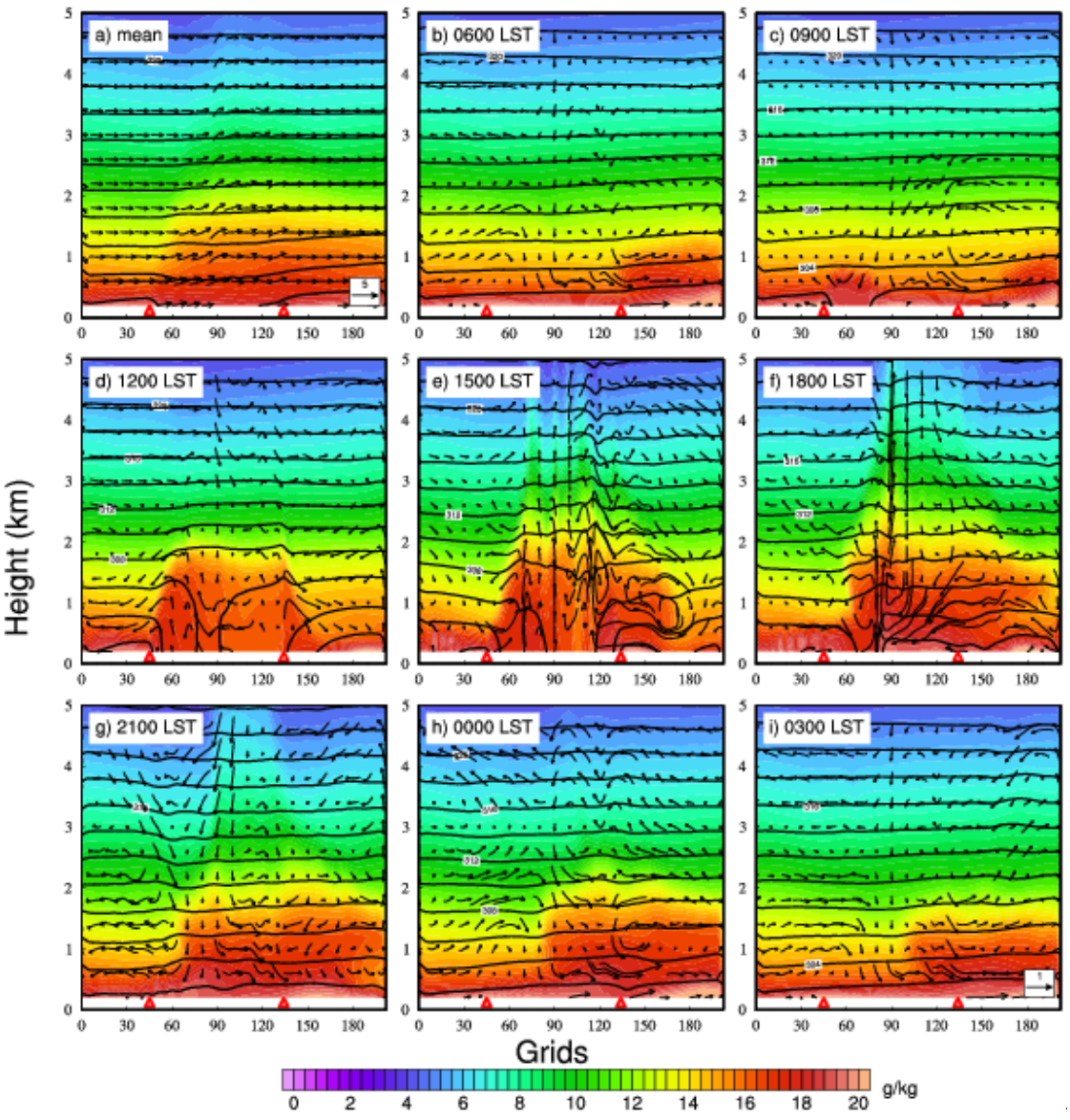
a) mean
b) 0600 LST
c) 0900 LST
d) 1200 LST
e) 1500 LST
f) 1800 LST
g) 2100 LST
h) 0000 LST
i) 0300 LST
Height (km)
Grids
0 30 60 90 120 150 180
0 1 2 3 4 5
0 2 4 6 8 10 12 14 16 18 20
g/kg

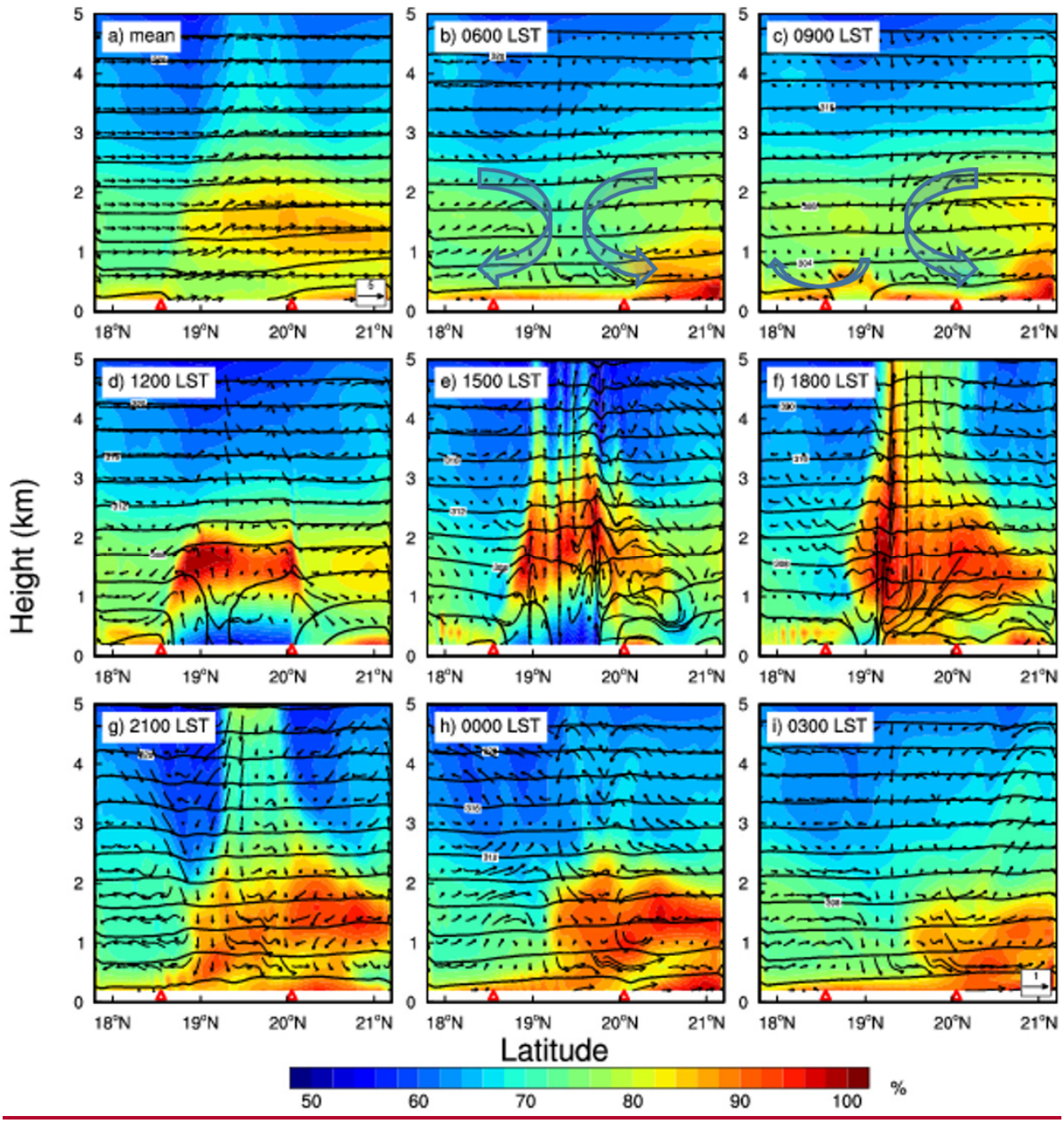

FIG. 14. Vertical cross-sections of ~~water vapor mixing ratio~~relative humidity (shading), perturbation wind (vectors; the scale of the vertical component is increased by a factor of 5), and temperature (contours) in the south-to-north direction (see red line in Fig. ~~1) averaged over all hours (a) and at 3-h intervals (b–i). The triangles in each panel indicate the edges of the island.~~

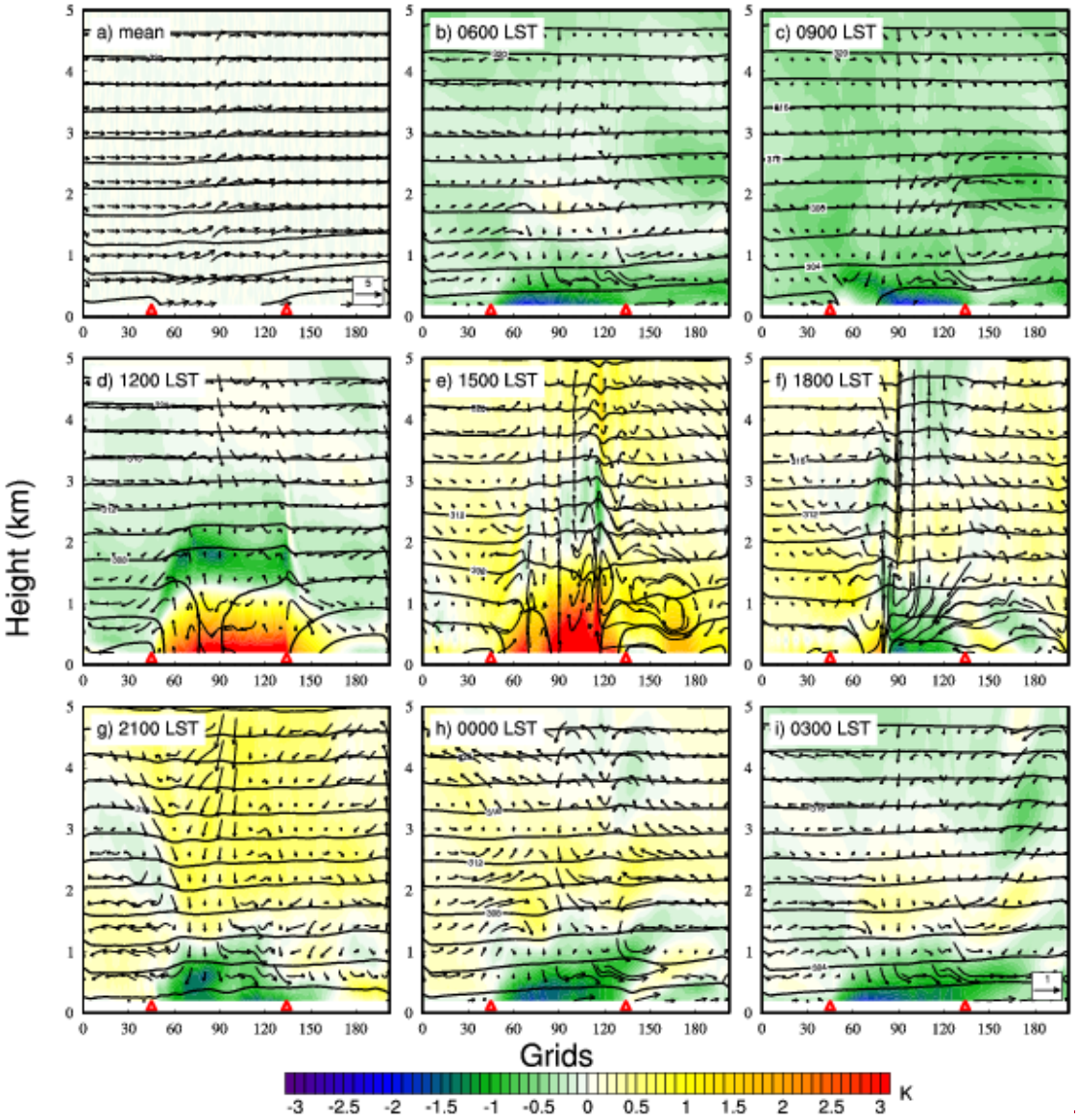

~~FIG.~~ ~~15. Vertical cross-sections of perturbation temperature (shading), perturbation wind (vectors; the scale of the vertical component is increased by a factor of 5), and temperature (contours) in the south-to-north direction (see red line in Fig.~~ 1) averaged over all hours (a) and at 3-h intervals (b–i~~).~~) in IDEAL simulation. The triangles in each panel indicate the edges of the island. Arrows in b and c stand for the land breeze circulations.

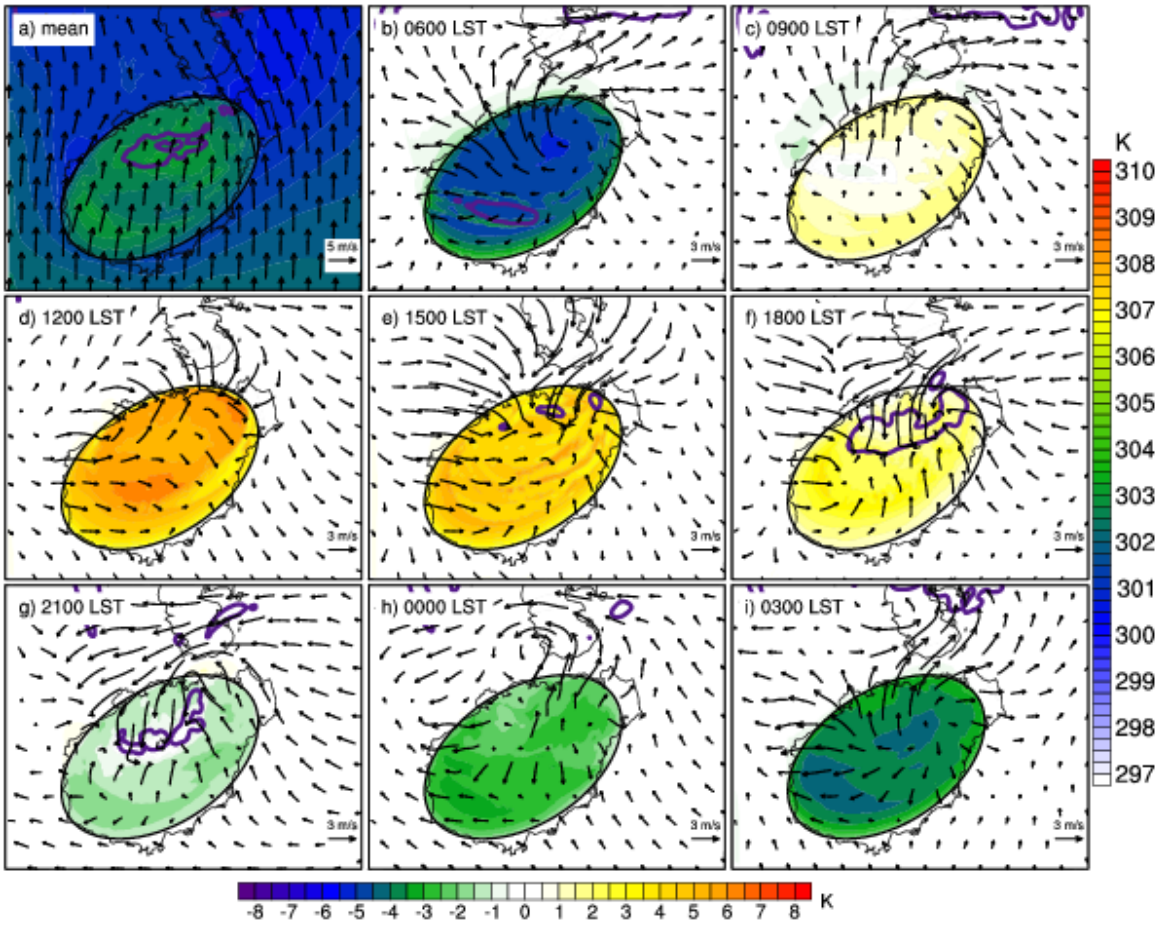
a) mean
b) 0600 LST
c) 0900 LST
d) 1200 LST
e) 1500 LST
f) 1800 LST
g) 2100 LST
h) 0000 LST
i) 0300 LST
5 m/s
3 m/s
K
310
309
308
307
306
305
304
303
302
301
300
299
298
297
-8 -7 -6 -5 -4 -3 -2 -1 0 1 2 3 4 5 6 7 8
K

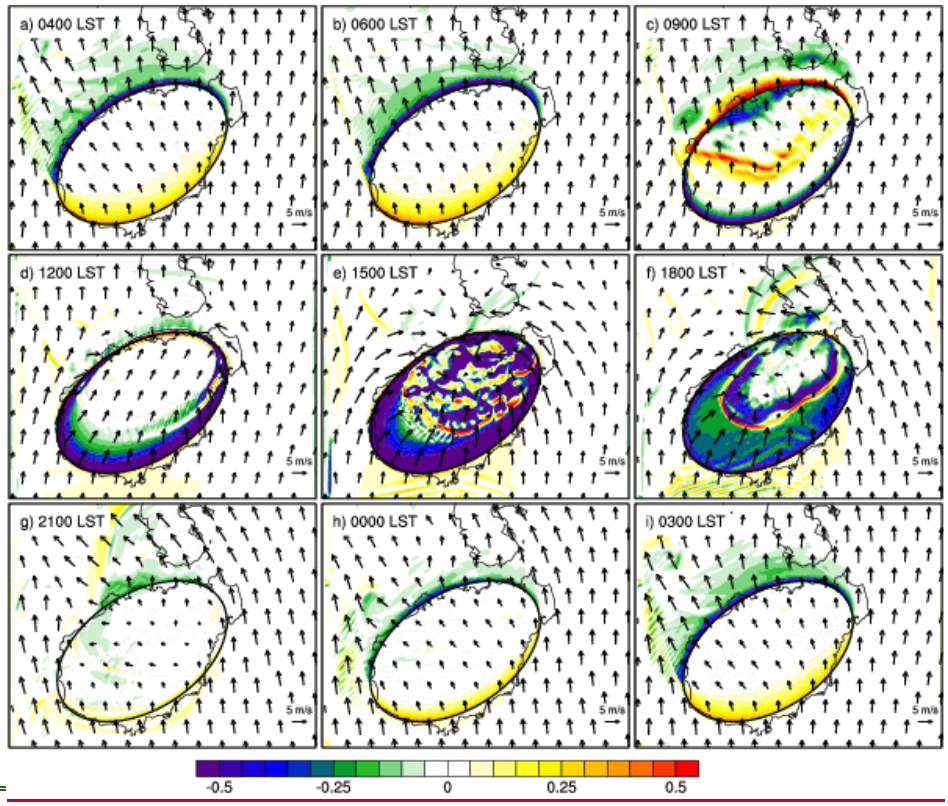

~~Fig.~~ FIG. 15. Horizontal temperature advection (shaded) and horizontal wind (vector, m s^{-1}) on the first model level in simulation IDEAL.

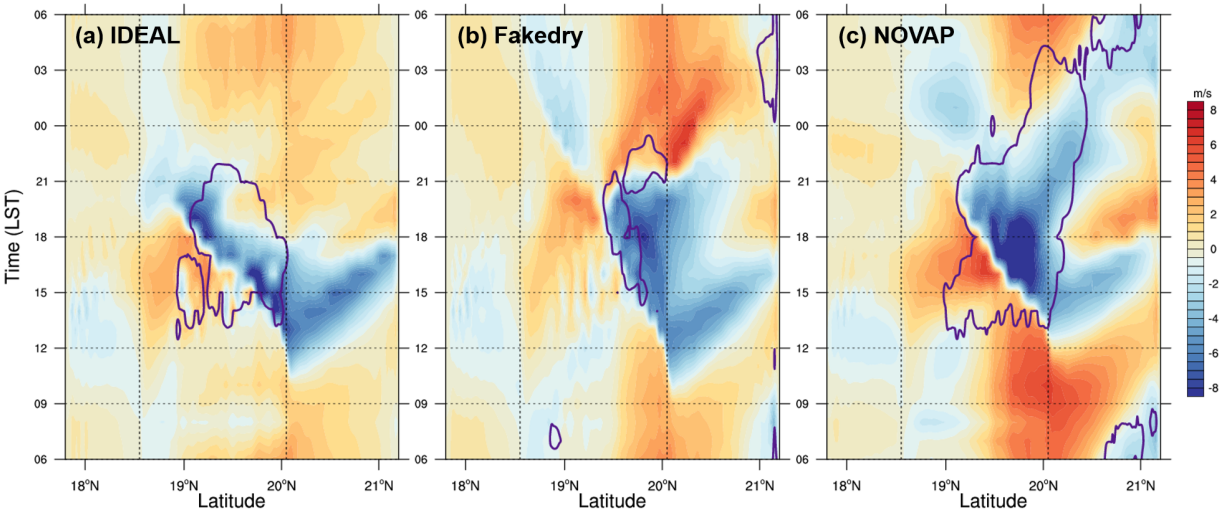

Fig. ~~16. As in Fig. 12, but for simulation Fakedry.~~

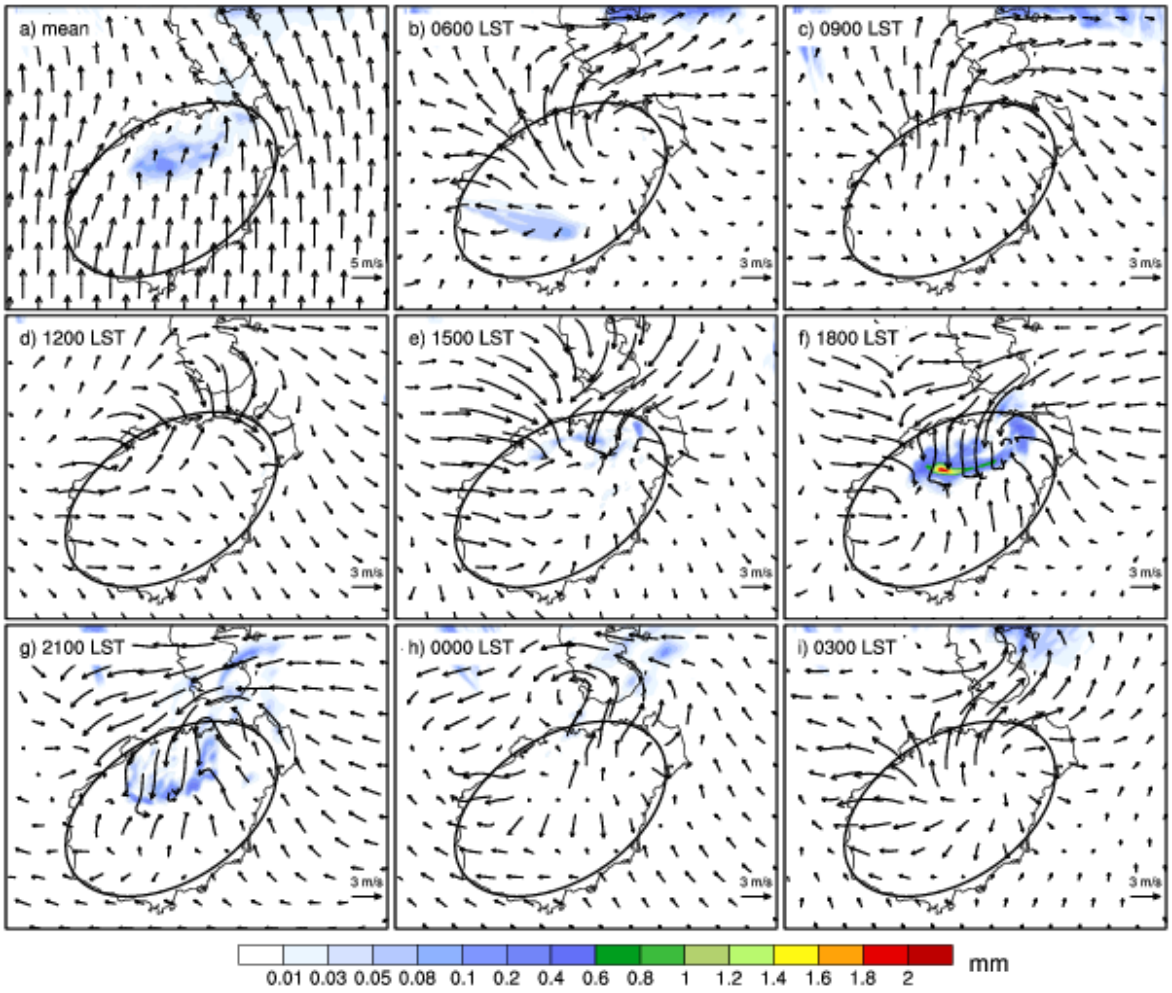

~~Fig. 17. As in Fig. 8, but for simulation Fakedry.~~

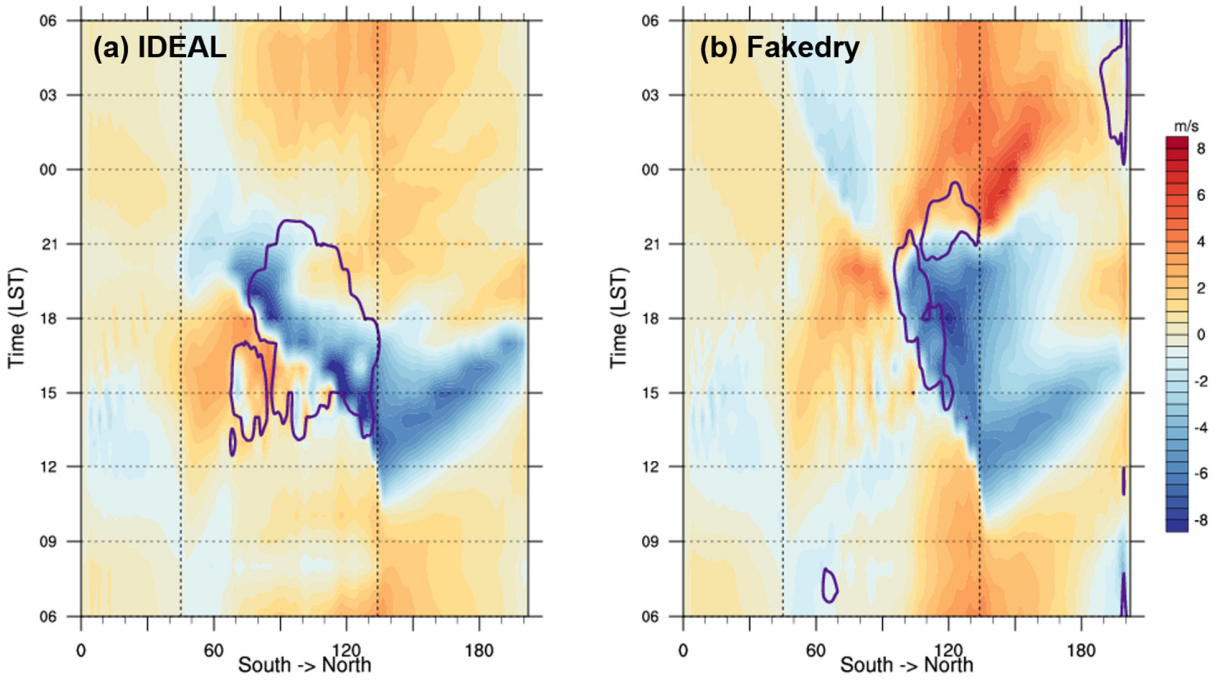

~~Fig. 18.~~16. Hovmoller diagrams of perturbation meridional wind component on the second lowest model level for horizontal wind (shading) in the (a) IDEAL ~~and~~, (b) Fakedry and (c) NOVAP simulations, respectively. Precipitation exceeding 0.1 mm h^{-1} is enclosed by the heavy purple contours. The two vertical dash lines indicate the edges of the island.

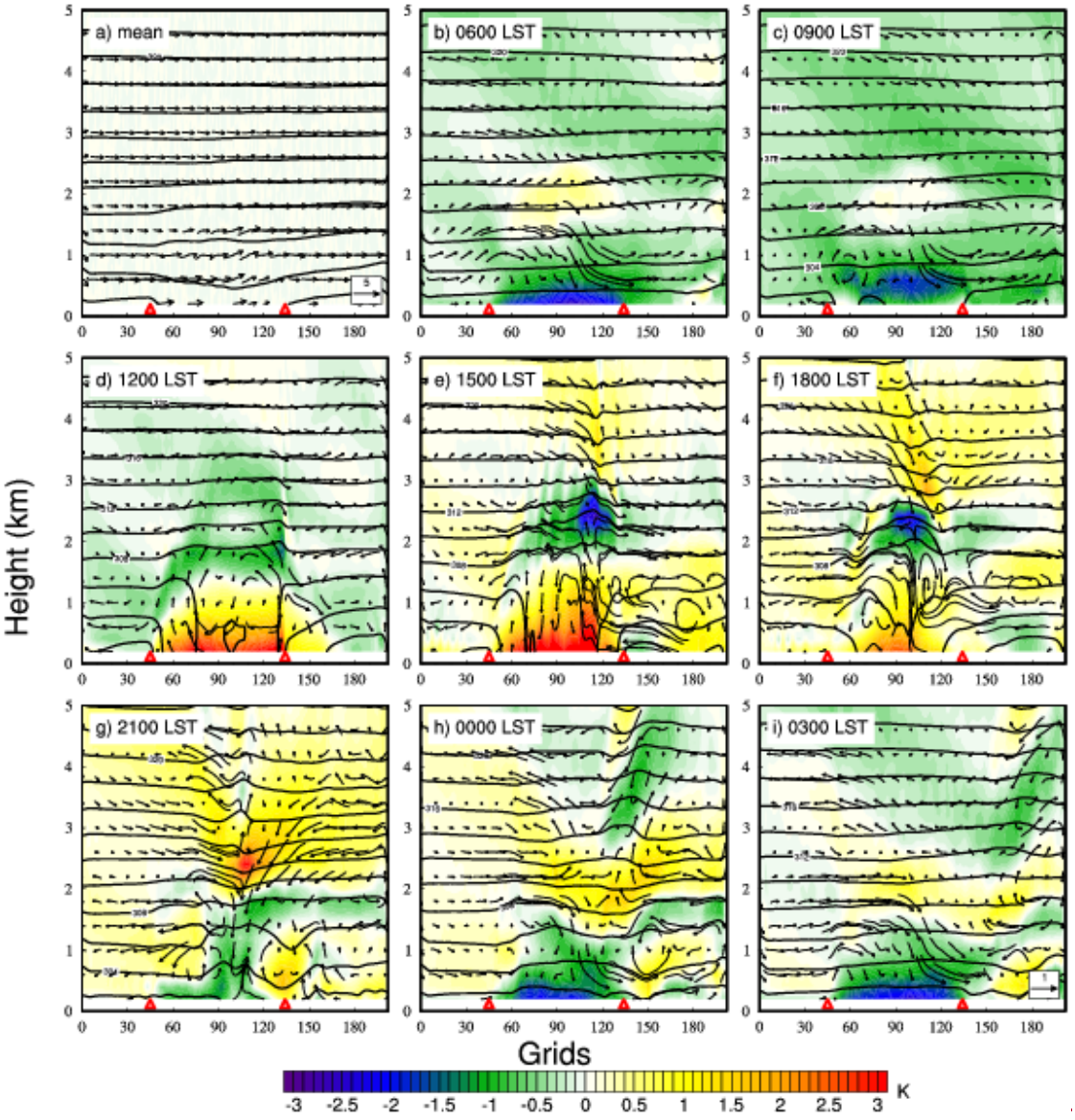

Fig. 19. As in Fig. 15, but for simulation Fakedry.